arXiv:1207.2476v1 [astro-ph.HE] 10 Jul 2012

Prepared for submission to JCAP
LUPM:12-039

Diffuse gamma-ray constraints on dark matter revisited
I: the impact of subhalos

Steve Blanchet[a] and Julien Lavalle[b]

[a]Institut de Théorie des Phénomènes Physiques, École Polytechnique Fédérale de Lausanne, CH-1015 Lausanne — SWITZERLAND
[b]Laboratoire Univers & Particules de Montpellier [LUPM] CNRS-IN2P3 / Université Montpellier II [UMR-5299] Place Eugène Bataillon - CC 72 F-34095 Montpellier Cedex 05 — FRANCE

E-mail: steve.blanchet@epfl.ch, lavalle@in2p3.fr

Abstract. We make a detailed analysis of the indirect diffuse gamma-ray signals from dark matter annihilation in the Galaxy. We include the prompt emission, as well as the emission from inverse Compton scattering whenever the annihilation products contain light leptons. We consider both the contribution from the smooth dark matter halo and that from substructures. The main parameters for the latter are the mass function index and the minimal subhalo mass. We use recent results from N-body simulations to set the most reasonable range of parameters, and find that the signal can be boosted by a factor ranging from 2 to 15 towards the Galactic poles, slightly more towards the Galactic anticenter, with an important dependence on the subhalo mass index. This uncertainty is however much less than that of the extragalactic signal studied in the literature. We derive upper bounds on the dark matter annihilation cross section using the isotropic gamma-ray emission measured by Fermi-LAT, for two directions in the sky, the Galactic anticenter and the Galactic pole(s). The former represents the lowest irreducible signal from dark matter annihilation, and the latter is robust as the astrophysical background, dominated by the hadronic contribution, is rather well established in that direction. Finally, we show how the knowledge of the minimal subhalo mass, which formally depends on the dark matter particle interactions with normal matter, can be used to derive the mass function index.

Keywords: Dark matter; Galactic diffuse gamma-ray emission; Galactic cosmic-ray transport

Contents

1 Introduction **1**

2 Astrophysical parameters: DM and target radiation fields in the Galaxy **4**

3 Gamma-ray emission **5**
- 3.1 Prompt gamma-ray contribution 5
- 3.2 Inverse Compton scattering 5

4 Transport of Galactic electrons **7**
- 4.1 Infinite 3D solution, and solutions with spatial boundaries 9
- 4.2 Asymptotic regimes: neglecting spatial diffusion or not 10
- 4.3 Attempts for modeling transport beyond the diffusion slab 12
- 4.4 Ascribing energy Losses 14

5 DM Subhalos **14**
- 5.1 Prompt emission 18
- 5.2 Inverse Compton 19

6 Results **19**

7 Conclusions **25**

1 Introduction

It is now well established that the dominant component of matter in the Universe is not conventional baryonic matter, but dark matter (DM) [1–3]. Moreover, it is also known that DM should be relatively *cold*, *i.e.* with a rather small free-streaming length at the matter domination period, in order to trigger the hierarchical formation of structures on time. The resulting cold dark matter (CDM) paradigm has been able to describe a wealth of data amazingly well, from galactic to cosmological scales. Prime among candidates to explain where DM stems from is the *weakly interacting massive particle* (WIMP). Its popularity arises from the simple fact that assuming a new particle with weak interactions and a mass around the electroweak scale automatically leads to the correct relic abundance, while providing specific and potentially observable signatures [4, 5]. This non-trivial result, as well as theoretical motivations for having new physics at the weak scale, converge to make this scenario very appealing. Nevertheless, the CDM paradigm might still suffer from predicting too much power on small scales, but this remains an open issue [6]. In turn, such a small scale power could be exploited for discovery purposes [7], as we will discuss below.

DM candidates arising in particle theories aimed at solving specific theoretical issues of the standard model (SM) are usually featured by the property of self-annihilation (or decay). This may be related to the stability of the proton, as is the case in the popular supersymmetric framework, and opens the possibility of detecting cosmic annihilation traces [5, 8–10]. DM indirect detection has been extensively studied in the past ten years, with a boost of activity since the successful launch of the latest gamma-ray satellite, the Fermi-LAT, granting a much higher sensitivity to point sources, a better energy resolution, and an energy range extending to higher energies than its predecessors [11]. In particular, the sensitivity to DM annihilation signals is better than ever, and probing cross sections lying in the canonical range fixed by requiring the correct WIMP cosmological abundance is now possible. However, after over 3 years of data taking, no signal was found which could be unequivocally traced back to DM, but a potential line-like feature around 130 GeV very recently found in the diffuse emission around the Galactic center [12, 13]. Since the latter remains to be inambiguously connected to DM, this conservatively implies that limits on DM model parameters could be extracted from the total observed gamma-ray flux. A non-exhaustive list of works using Fermi-LAT results is [14–24]. These studies differ in that the gamma-ray signal from DM annihilation was inferred either from the Galactic, extragalactic, or both contributions. Moreover, different sets of data were considered, namely different directions in the sky or the isotropic diffuse gamma-ray background [25]. Here we would like to focus on the contribution coming from the Galactic halo only so as to minimize the theoretical uncertainties; we leave the extragalactic calculation for a future work. Note that, except for extreme astrophysical assumptions, the Galactic component usually provides more stringent constraints than the extragalactic one [19, 20].

In the works cited above, the treatment of the DM-induced photon emission typically suffers from the following shortcomings:

- For final states involving charged leptons, the diffusion of subsequent electrons and positrons from the point of annihilation to the point where they produce gamma-rays by inverse Compton (IC) scattering is neglected.
- DM substructures, which are expected to populate the Galactic halo in number, are neglected.

Regarding the first point, the diffusion of electrons is typically assumed to be negligible away from the galactic center when computing the gamma-ray flux from DM annihilation. Intuitively, this might only be correct when the density gradient is small over large enough distances, larger than the typical diffusion length. This was verified to some extent in [26] (see also [15]), but focusing mostly on regions where the locally constrained diffusion coefficient is still meaningful. This therefore mostly concerns the so-called diffusion zone. Nevertheless, DM annihilation also injects cosmic-ray (CR) electrons outside this region, which should also contribute to the overall IC gamma-ray production along the line of sight. Here, we will shortly discuss this statement further, and see to what extent the approximation of neglecting spatial diffusion holds. We will perform a full analysis of the transport issue in a subsequent paper.

Moreover, subhalos are predicted by structure formation, either in full analytic approaches of hierarchical clustering such as spherical [27] or ellipsoidal collapse [28], and in N-body numerical simulations (for recent examples, see Via Lactea II [29] or Aquarius [30]), although the resolution needed to probe the smallest scales within the WIMP paradigm is out of reach, except at very large redshifts [31].

The fact that DM is not uniformly distributed across the Universe and forms halos (and subhalos) has obviously already been included in early works on the DM-induced extragalactic gamma-ray emission and its possible detection [32]. Missing this part would have led to underestimate the related flux by a factor of at least 10^4. As for the DM signal from within our Galaxy, it was also realized a long time ago that subhalos could play an important role [7, 33, 34]. However, in recent years the tendency in DM indirect detection with gamma-rays was often to neglect this effect altogether (except in a few cases [18, 19, 26]), although, ironically enough, it is likely subject to less theoretical uncertainty than the extragalactic counterpart.

Within the CDM paradigm, our Galactic halo is big enough to expect a large number of DM clumps populating it. Large N-body simulations already see tens of thousand of them down to their resolution [35]. A conservative extrapolation would then imply that the number of clumps populating our Galaxy is of the order of, or larger than 10^{13} for Earth-mass objects. It is well known that the presence of Galactic subhalos must increase the diffuse Galactic emission at large latitudes, though the amplification is expected to be modest, less than a factor of 10 typically [26]. Nevertheless, given the current constraints, essentially on small WIMP masses around 10 GeV or so, a factor of a few may have an important impact on still allowed borderline configurations. In order to have a robust and realistic prediction for the gamma-ray flux on Earth, it is then crucial to include subhalos in a consistent way. This is another goal of ours for this paper.

It is important to discuss which data sets and directions in the sky should be preferred in order to derive robust bounds on the annihilation cross section. Clearly, the total gamma-ray flux measured by Fermi-LAT in every direction in the sky is a possible choice, but it is most probably too conservative. Indeed the conventional Galactic diffuse component induced by astrophysical CRs makes up a prominent part (if not most) of the total measured flux. The Fermi collaboration has actually recently released an extensive work addressing the CR-induced Galactic diffuse emission in detail [36]. We note that the main contribution comes from hadronic processes involving CR nuclei (mostly protons) and the interstellar gas, while a subdominant one comes from the IC scattering of CR electrons off the interstellar photon field (including the cosmic microwave background — CMB). Besides, the former is subject to less uncertainty than the latter. Moreover, we have a large number of (extragalactic) astrophysical sources (mainly blazars) which feature a substantial fraction of the total flux. Subtracting the galactic diffuse emission and the emission from known sources from the total flux was one of the many important contributions by the Fermi collaboration [25], leading to a residual component found isotropic, the so-called diffuse isotropic gamma-ray background (IGRB). In this work, we will use this estimate of the IGRB to set limits on DM annihilation cross-sections. Although doing so exposes us to the modeling used by the Fermi collaboration to subtract the galactic diffuse emission, we are confident that in the direction of the Galactic poles (GPs), the IGRB offers a robust upper limit for any gamma-ray flux from DM annihilation. We will also calculate fluxes in the direction of the Galactic anticenter (GAC), because it is the smallest possible gamma-ray flux and therefore acts as an irreducible isotropic component. However, in this direction, the subtraction of the Galactic diffuse emission by the Fermi collaboration is more uncertain, as we will discuss.

This paper is organized as follows. In Sect. 2 we introduce the main definitions, and provide some important astrophysical parameters that will be used in the remainder of the paper. In Sect. 3, we present the different sources of gamma-rays stemming from DM annihilation (prompt and IC), and provide the formulæ used to compute gamma-ray fluxes on Earth in any direction in the sky. Sect. 4 is devoted to the transport of electrons and positrons in the Galaxy. Sect. 5 shows how Galactic subhalos can be self-consistently included within the calculation of gamma-ray fluxes. We finally present our main results in Sect. 6, and draw our conclusions in Sect. 7.

	CMB	IR	SL
T_i [eV]	2.35×10^{-4}	2.85×10^{-3}	2.8×10^{-1}
$n_i^0/n_i^{\rm bb}$	1	4.5×10^{-5}	7×10^{-13}

Table 1: ISRF temperatures and density normalizations with respect to the blackbody reference values.

2 Astrophysical parameters: DM and target radiation fields in the Galaxy

The DM halo of our Milky Way (MW) may be well described by the so-called Navarro-Frenk-White (NFW) profile [37]

$$\rho(r) = \frac{\rho_s}{r/r_s(1+r/r_s)^2}\,, \tag{2.1}$$

where r_s is the scale radius, and ρ_s is the scale density. In the following, we will use the parameters determined in a recent study of the Galactic kinematic data [38], namely a scale radius of 20.2 kpc, a local density of $\rho_\odot = 0.395$ GeV/cm^3, and a Sun-GC distance of $r_\odot = 8.29$ kpc, which, put together, fix the scale density given above. These parameters are in agreement with those found in other complementary works [39–41].

The interstellar radiation field (ISRF), which defines the target photons for IC scattering, is made of three main components [42]: starlight (SL), infrared (IR) light emitted by the interstellar gas, and the CMB. We assume these components to obey blackbody distributions such that the differential number density for any kind i reads:

$$\frac{{\rm d}n_i}{{\rm d}E}(E,r',z) = n_i^0\, f(r',z)\frac{E^2}{\pi^2}\frac{1}{\exp(E/T_i)-1}\,, \qquad i = {\rm SL, IR, CMB} \tag{2.2}$$

where (r',z) are cylindrical coordinates centered on the Sun's position, and, except for the CMB for which $f(r',z) = 1$, we follow Ref. [43] for the parameterization of the position dependent normalization:

$$f(r',z) = \exp\left[-\left(r'/r_{\rm ph} + |z|/z_{\rm ph}\right)\right]\,, \tag{2.3}$$

with $r_{\rm ph} = 3.2$ kpc and $z_{\rm ph} = 0.4$ kpc. The normalizations as well as reference temperatures T_i are given in Tab. 1.

We further account for the presence of a magnetic field in the Galaxy which enters the electron energy losses (see Sect. 4.4), the energy density of which can be expressed as:

$$\begin{aligned} u_B(r,r) &= \frac{B^2(r,z)}{8\pi}\,, \\ B(r,z) &= B_\odot \exp\left(-\frac{(r-r_\odot)}{r_B} + \frac{|z|}{z_B}\right)\,. \end{aligned} \tag{2.4}$$

We normalize the magnetic field to a local value of $B_\odot = B(r = r_\odot, z = 0) = 3\ \mu$G. This corresponds to a magnetic field of $\sim 7\ \mu$G at the GC. Following [44] we choose typical values of $r_B = 10$ kpc and $z_B = 2$ kpc.

3 Gamma-ray emission

3.1 Prompt gamma-ray contribution

If DM annihilates into charged particles, photons may be emitted in two ways, which we collectively refer to as *prompt* emission: (i) if the final state particles hadronize, they will produce neutral pions which decay into photons; (ii) charged particles will radiate photons from internal Bremsstrahlung processes [45]. In the following, we will assume that DM is made of Majorana particles, denoted χ. The prompt photon flux collected on Earth from DM annihilation in the Galactic halo, along a line of sight (los) ds and within a solid angle $\delta\Omega_{\rm res}$ is given by

$$\frac{{\rm d}\Phi}{{\rm d}E_\gamma} = \frac{r_\odot}{4\pi} \left\{ \mathcal{S} \equiv \frac{\langle\sigma v\rangle}{2} \frac{\rho_\odot^2}{m_\chi^2} \right\} \frac{{\rm d}N_\gamma}{{\rm d}E_\gamma} \int_{\delta\Omega_{\rm res}} {\rm d}\Omega \int_{\rm los} \frac{{\rm d}s}{r_\odot} \left(\frac{\rho(r)}{\rho_\odot} \right)^2 , \tag{3.1}$$

where ${\rm d}N_\gamma/{\rm d}E_\gamma$ is the photon spectrum per annihilation, $\langle\sigma v\rangle$ is the thermally averaged annihilation cross-section, and the density profile is given in Eq. (2.1). The galactocentric radius r can be expressed in terms of the line-of-sight distance s and the galactic coordinates (b, ℓ):

$$r(s) = \sqrt{r_\odot^2 - 2\, s\, r_\odot\, \cos(\ell)\, \cos(b) + s^2}\,. \tag{3.2}$$

3.2 Inverse Compton scattering

The most recent analyses focussed on DM models which couple dominantly to the lepton sector (see *e.g.* [15, 16, 20, 46, 47]). Such models may account for the rising positron fraction observed by the PAMELA experiment [48], and in some cases the electron-positron spectral feature found around a few hundreds of GeV with the Fermi-LAT instrument [49]. However, it must be kept in mind that such scenarios will typically produce an overabundance of photons as well, due to inverse Compton scatterings from final-state electrons and positrons [1]. It is then a quantitative question whether such models are excluded or not, and many groups have contributed to this discussion [15–17, 19–21].

The photon energy spectrum arising from the inverse Compton scattering of an incoming electron of energy E (and Lorentz factor $\gamma_e = E/m_e$) off an incoming photon of energy $E_{\rm in}$ is given by [50–52]

$$\begin{aligned} \mathcal{P}_i(E_\gamma, E, \vec{x}) &= \frac{3\sigma_T\, c}{4\gamma_e^2} \int_{1/4\gamma_e^2}^{1} {\rm d}q\, \frac{1}{q} \frac{{\rm d}n_i}{{\rm d}E_{\rm in}}(E_{\rm in}(q), \vec{x})\, f(q)\,, \\ f(q) &= 1 + 2q \left\{ \log q - q + \frac{1}{2} \right\} + \frac{(1-q)}{2} \frac{(\Gamma_e q)^2}{1 + \Gamma_e q}\,, \end{aligned} \tag{3.3}$$

where $q = \frac{E_\gamma}{\Gamma_e(E - E_\gamma)}$, $\sigma_T = 0.665$ barn is the Thomson cross section, $\Gamma_e = 4E_{\rm in}\gamma_e/m_e$ is a dimensionless parameter that determines the regime of the scattering, *e.g.* the Thomson limit when $\Gamma_e \ll 1$. We show in Fig. 1 how this function depends on the energy of the outgoing photon E_γ, and on the incoming electron energy E. As explained in Sect. 2, the target photons here can be the CMB, IR light or starlight, represented by the subscript i

---

[1] For our purposes, the fact that electrons and positrons have a different charge has no importance, and therefore, from now on, we will refer to *electrons and positrons* as simply *electrons*.

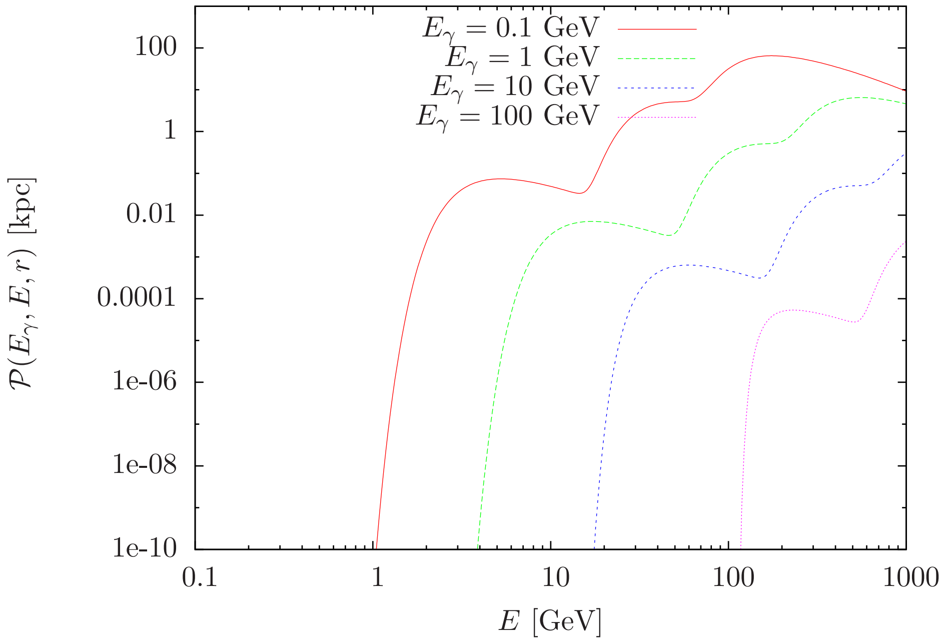

Figure 1: Differential photon power emitted by an electron of energy E.

in Eq. (3.3). In Fig. 1, we plot the total photon spectrum, which is the sum of these three components, appearing in the figure as bumps, the leftmost one originating from electrons scattering off the CMB, the middle one off IR, and the rightmost one off SL. These bumps unveil the initial target photon distributions (taken thermal here), and feature the original peaks, initially around $E_{\rm in} \approx T_i$, which have been IC-upscattered to energy $E_\gamma \approx \gamma_e^2 T_i$. One can then express the photon flux on Earth due to such processes, as observed in a solid angle $\delta\Omega_{\rm res}$, given a differential electron number density $\mathcal{N}_e(\vec{x}, E) \equiv dn_e/dE$:

$$\frac{{\rm d}\Phi}{{\rm d}E_\gamma} = \frac{r_\odot}{4\pi} \int_{\delta\Omega_{\rm res}} {\rm d}\Omega \int_{\rm los} \frac{{\rm d}s}{r_\odot} \int_{m_e}^{m_\chi} {\rm d}E \, \mathcal{N}_e(\vec{x}(s,\theta,\phi), E) \sum_i \mathcal{P}_i(E_\gamma, E, \vec{x}(s,,\theta,\phi)) \,. \tag{3.4}$$

In order to calculate the photon flux from IC scattering, one therefore needs to know the electron number density produced from DM annihilation along the line of sight s. We will show how to calculate this density everywhere in the galaxy in Sect. 4, taking into account spatial diffusion effects. We note that Eq. (3.4) implicitly assumes that the incoming electron and photon fluxes are isotropic at position $\vec{x}$, which should be questioned in the present context. We will shortly discuss this in Sect. 4, but we will dedicate a more complete study of this issue in a forthcoming paper.

We show in Fig. 2 the prompt/IC spectra associated with different masses of WIMPs annihilating into e^+e^- for two different lines of sight: the Galactic anticenter (GAC) and the Galactic pole(s) (GP). These spectra correspond to the energy integral of Eq. (3.4), normalized to the local annihilation rate $\mathcal{S}$ defined in Eq. (3.1):

$$\frac{{\rm d}N_\gamma^{\rm IC}(s,b,\ell)}{{\rm d}E_\gamma} = \frac{1}{\mathcal{S}} \int_{m_e}^{m_\chi} {\rm d}E \; \mathcal{N}_e(\vec{x}(s,b,\ell), E) \sum_i \mathcal{P}_i(E_\gamma, E, \vec{x}(s,b,\ell)) \,. \tag{3.5}$$

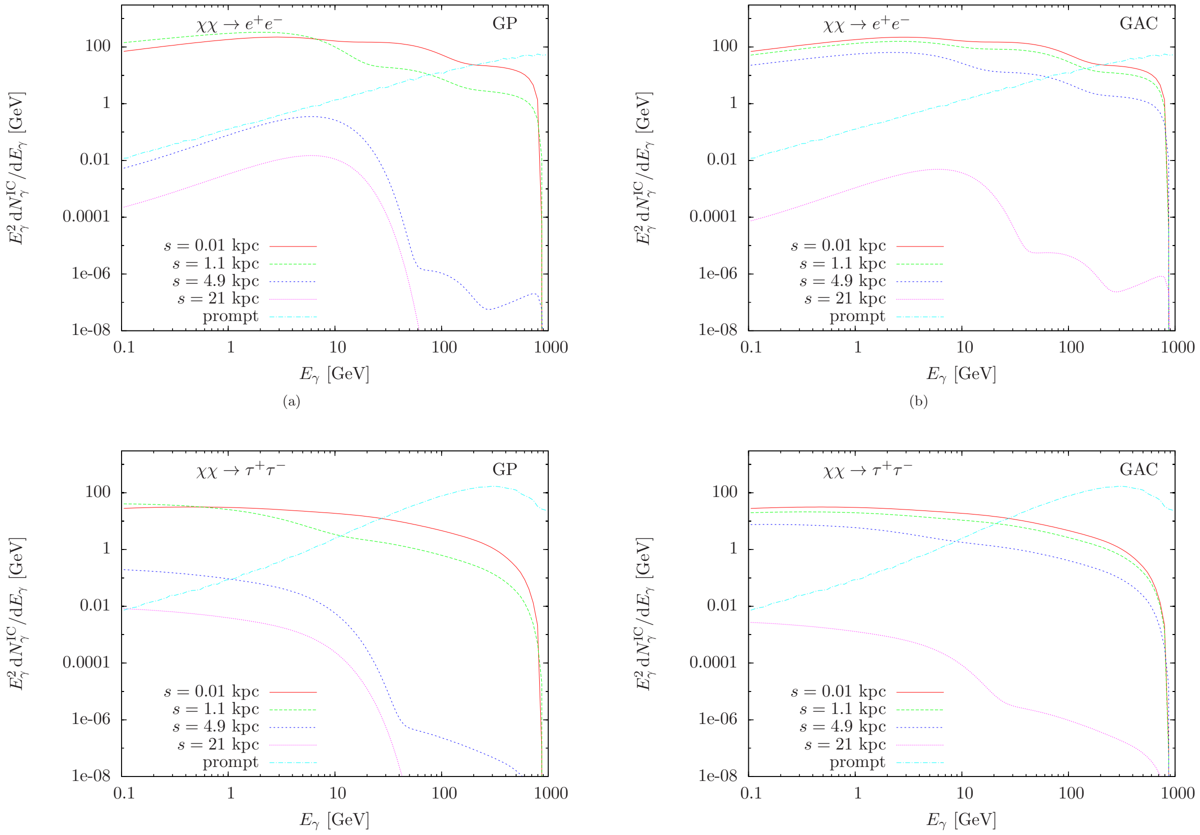

(a) (b) (c) (d)

Figure 2: Differential photon spectrum produced for a 1 TeV DM particle annihilating into e^+e^- (top) and $\tau^+\tau^-$ (bottom). The IC contribution is shown at different distances on the l.o.s. towards the GP (left) and the GAC (right) and the prompt contribution is shown as a reference.

It can be seen that the spectrum drops quite dramatically at high energies for the GP because the target photon density decreases fast as one goes away from the Galactic disk (see next section). The CMB being present everywhere, its bump is only affected by the smaller energy losses away from the Galactic center. Increasing the distance towards the GAC also shows a decrease in the high-energy spectrum, but to a much lesser extent than the GP. One can also notice that the prompt component starts dominating at the high-energy end of the spectrum, as expected. DM annihilation into $\tau^+\tau^-$ exhibits the same features. The main differences are: 1) the IC spectrum is shifted to lower energies and *smeared* because the electron energy distribution is not as sharp as the e^+e^- case; 2) the prompt component is more dominant here because τ can decay hadronically producing many more photons. We have made use of the Pythia Monte Carlo generator [53] to compute the injected electron spectra in all cases.

4 Transport of Galactic electrons

Electrons produced from DM annihilation may scatter off Galactic magnetic inhomogeneities, which induces a diffusive motion, and lose energy mostly through synchrotron and inverse

Compton (IC) processes in the energy range considered here. These losses give rise to the broad electromagnetic spectrum that may help, in turn, trace or constrain the electron distribution, from radio frequencies (synchrotron) to gamma-rays (IC), and which we are interested in in this paper. In order to calculate the differential electron number density at all times and positions, one needs to solve a diffusion-loss equation [54–56]. Neglecting convection and reacceleration, which become sizable only below a few GeV [57], the diffusion-loss equation for electrons reads

$$\partial_t \mathcal{N}(E,\vec{x}) - \vec{\nabla}\left\{K(E,\vec{x})\,\vec{\nabla}\mathcal{N}(E,\vec{x})\right\} - \partial_E\left\{b(E,\vec{x})\mathcal{N}(E,\vec{x})\right\} = \mathcal{Q}(E,\vec{x})\,, \tag{4.1}$$

where $\mathcal{Q}$ is the electron source term, and diffusion on magnetic turbulences is described with a diffusion coefficient $K(E,\vec{x})$ which is energy and *a priori* spatial dependent. The energy losses $b(E,\vec{x}) = -dE/dt$ are also spatial dependent since, beside including the CMB, they are characterized by interactions with the magnetic field and the interstellar radiation field — energy losses are discussed into more detail in Sect. 4.4. In this paper, the source term is proportional to the squared DM density (assuming Majorana WIMPs):

$$Q(E_s,\vec{x}_s) = \mathcal{S}\left[\frac{\rho(\vec{x}_s)}{\rho_\odot}\right]^2 \frac{\mathrm{d}N_e}{\mathrm{d}E_s}\,, \tag{4.2}$$

where the local annihilation rate $\mathcal{S}$ was defined in Eq. (3.1). We note that when subhalos are included — see Sect. 5 — the source can be split into two separate terms [34]. The first one regards the smooth halo component, and corresponds to Eq. (4.2) with the substitution $\rho \to \rho_{\rm sm}$. The second one, which will be fully derived in Sect. 5 (all relevant definitions will be found there), reads

$$Q_{\rm sub}(E_s,\vec{x}_s) = \mathcal{S}\,\bar{N}_{\rm cl}\,\langle\xi(r)\rangle_M\,\frac{d\mathcal{P}_V(r)}{d^3\vec{x}_s}\,\frac{\mathrm{d}N_e}{\mathrm{d}E_s}\,. \tag{4.3}$$

Since the source is stable over cosmological times, one can safely take the steady state limit of Eq. (4.1), which can be solved either numerically (*e.g.* [22, 58, 59]), or, given some approximations, with semi-analytic methods (*e.g.* [34, 43, 60, 61]).

The difficulty arising in predicting the IC contribution to the diffuse gamma-ray flux is to estimate the electron distribution far away from the Galactic disk. Indeed, most of propagation models are usually based on the assumption that the cosmic-ray density vanishes at a certain distance from the Galactic plane, which is accounted for by imposing spatial boundary conditions when solving Eq. (4.1). This is actually an empirical way to describe the transition between diffusion and ballistic motion: when cosmic rays reach the spatial boundaries, they cannot, in principle, be scattered backward anymore by magnetic inhomogeneities, which should have also vanished. This assumption has been used in transport models in which the diffusion coefficient is taken homogeneous in a zone significantly more extended than the Galactic disk to deal with the escape of standard cosmic rays from the Galaxy, the sources of which are confined in the disk. Although the diffusion coefficient should in principle be related to the magnetic turbulence [62, 63], and hence likely be anisotropic and inhomogeneous, these simplified and minimal transport models still provide powerful tools to understand the physics at stake, and a rather good description of current cosmic-ray and diffuse gamma-ray data.

While the physical relevance of the spatial boundary conditions can be questioned in the present context, an additional difficulty comes with the estimate of the effective size of the diffusion zone. Accurate values are somewhat hard to extract from cosmic-ray data because of the well known degeneracy with the diffusion coefficient. Nevertheless, recent analyses and discussions suggest that the most critical one, the vertical half-width of the diffusion zone L, should be $\gtrsim 4$ kpc [25, 36, 64–66]. This value is critical for predicting the *local* cosmic-ray density originating in DM annihilation, since it defines the size of the region inside which diffusion is efficient enough to confine the injected particles [66, 67]. Nevertheless, as soon as one is interested in predicting the cosmic-ray distribution over larger scales, especially when the sources spread away from the diffusion zone, such a treatment could be inappropriate, since it imposes that the cosmic-ray density is null on the spatial boundaries and outside: this is obviously not case for DM-induced cosmic rays, which are expected to be injected all over the dark halo — still, the local impact of this *outside* zone is expected to be weak, unless for very intense sources. Here, including all cosmic-ray electrons is particularly important to derive IC constraints, since the target CMB photons are homogeneously spread all over the dark halo.

In the following, we will discuss different potential solutions to Eq. (4.1) that may arise in the context of DM annihilation. To do so, we may assume that any solution can be expressed in the form of a Green function $\mathcal{G}$ such that the differential electron density $\mathcal{N}$ can be calculated from

$$\mathcal{N}(E,\vec{x}) = \int_{E_s=E}^{E_s=\infty} \mathrm{d}E_s \int \mathrm{d}^3\vec{x}_s\, \mathcal{G}(E,\vec{x} \leftarrow E_s,\vec{x}_s)\, Q(\vec{x}_s,E_s)\,. \tag{4.4}$$

Such a Green function can then be interpreted as the probability for an electron injected at position $\vec{x}_s$ with energy E_s to diffuse to position $\vec{x}$ down to energy $E < E_s$.

4.1 Infinite 3D solution, and solutions with spatial boundaries

Assuming that the diffusion coefficient and the energy losses are homogeneous inside the whole Galaxy, which is certainly wrong except for losses due to IC scattering off the CMB, and forgetting about any boundary condition for the moment, one can recast Eq. (4.1) into the well-known inhomogeneous heat equation, the solution of which is easily derived [54]. In an infinite 3D space, the associated Green function is given by

$$\mathcal{G}(E,\vec{x} \leftarrow E_s,\vec{x}_s) = \frac{1}{b(E)\,(\pi\,\lambda^2)^{3/2}} \exp\left\{-\frac{|\vec{x}-\vec{x}_s|^2}{\lambda^2}\right\}\,, \tag{4.5}$$

where λ, a function of energy, can be interpreted as the electron propagation length and carries the dimension of a distance. It reads

$$\lambda^2(E,E_s) = 4\int_E^{E_s} \mathrm{d}E' \frac{K(E')}{b(E')}\,. \tag{4.6}$$

This integral is analytic when Klein Nishina effects are neglected. As we will show in the following, λ plays a crucial role in the phenomenology of electron propagation. We note that when $\lambda \to 0$, we reach an asymptotic regime which corresponds to neglecting spatial diffusion (the energy loss timescale is much shorter than the diffusion timescale). Nevertheless, we emphasize that this asymptotic regime may be associated with two distinct physical situations: (i) the diffusion coefficient is vanishingly small, in which case electrons lose their energy while being stuck at the same position; (ii) the electron energy of interest is very close to the injected energy — see Sect. 4.2.

In most of propagation models, cylindrical symmetry is assumed, based on the observed morphology of spiral galaxies at different wavelengths, and both radial and vertical boundaries, where the cosmic-ray density is assumed to vanish, help define the spatial extent of the diffusion zone. For the MW, the former is taken around $R \approx 20 - 30$ kpc, while the latter $L \approx 5$ kpc. Inside this slab, the diffusion coefficient is generally taken homogeneous and isotropic. This may appear contradictory with the fact that diffusion is driven by cosmic-ray interactions with magnetic turbulences, and should consequently be closely related to the Galactic magnetic field configuration, but in the absence of a yet full theoretical understanding of this process, simplicity is fairly motivated. We will not recall the full set here, but note that when energy losses are assumed fully homogeneous, semi-analytic solutions to Eq. (4.1) do exist in the form of Green functions or Fourier-Bessel expansions (*e.g.* [34, 60, 61, 68, 69]). When parts of the energy losses and sources can be assumed as fully confined in the disk, some tricks can be used to accurately predict the local density of electrons *at the Earth* [43, 57]. When energy losses have a more complicated spatial distribution, then it is difficult to avoid a full numerical treatment, unless specific energy range or spatial distributions of the relevant ingredients (including the source) are considered [43].

4.2 Asymptotic regimes: neglecting spatial diffusion or not

As introduced above, an interesting asymptotic regime arises when the propagation length $\lambda \to 0$. This actually amounts to compare two different timescales, the energy loss timescale and the spatial diffusion timescale, which can respectively be written as:

$$\begin{aligned} \tau_l(E, E_s, \vec{x}) &= \int_E^{E_s} \frac{dE'}{b(E', \vec{x})} \approx \frac{E}{b(E, \vec{x})} \\ \tau_d(E, \vec{x}) &= d^2 / K(E, \vec{x}) \, , \end{aligned} \tag{4.7}$$

where d is either the distance to the source or the scale of interest, and where we have indicated the potential spatial dependence in both cases. Note that the approximation made in the first line for τ_l is only valid for $E \ll E_s$. Therefore, the asymptotic condition can be re-expressed in terms of a relation between energy and distance:

$$\begin{aligned} \tau_l(E, E_s, \vec{x}) &\ll \tau_d(E, \vec{x}) \\ d^2 &\gg E\, K(E, \vec{x}) / b(E, \vec{x}) \approx \lambda^2(\vec{x}) \, . \end{aligned} \tag{4.8}$$

The distance d then characterizes the spatial scale for which neglecting spatial diffusion is a good approximation. We see that it depends on energy, and we actually recover the scale λ discussed above, as expected. To get more physical insight, we can take the Thomson approximation for the energy losses, with $\tau_l(E) \approx 10^{16}\text{s}(E/\text{GeV})^2$ (gross estimate valid at the solar position), and a typical value of $K(E) \approx 0.01\,\text{kpc}^2/\text{Myr}\,(E/\text{GeV})^{0.7}$. We find that this regime is valid for scales:

$$d \gg 1.8\,\text{kpc}\,(E/\text{GeV})^{-0.15} \, .$$

As expected from the energy loss behavior, we therefore clearly see that this specific regime is only valid either at very high energies, or at very low diffusion coefficient; unless the source itself exhibits a negligible spatial gradient within a volume of typical length d, in which case spatial diffusion is irrelevant. This was already emphasized in [70] in the context of Sunyaev-Zel'dovich calculations. Therefore, this approximation becomes reliable in regions where the magnetic field could be very large, like in the Galactic center, but this does not concern the present study. For completeness, let us write the Green function associated with this specific regime:

$$\mathcal{G}_{\not{K}}(E,\vec{x} \leftarrow E_s,\vec{x}_s) = \frac{\delta^3(\vec{x}-\vec{x}_s)}{b(E,\vec{x})}\,, \tag{4.9}$$

such that the electron density originating in DM annihilation gets a very simple analytic expression:

$$\mathcal{N}_{\not{K}}(E,\vec{x}) = \frac{1}{b(E,\vec{x})}\int_E^{\infty} \mathrm{d}E_S\,\langle \mathcal{Q}(E_S,\vec{x})\rangle_d\,. \tag{4.10}$$

The symbol $\langle\rangle_d$ means that the source term $\mathcal{Q}$ featuring this equation has to be understood as an average over the relevant scale d over which the approximation is valid. We note that such an approximation has often been used to predict the electron density outside the diffusion zone, to further compute IC contributions to the diffuse gamma-ray flux in the absence of a complete and self-consistent transport model (*e.g.* [14, 15, 17, 20, 71]). We emphasize that this is erroneous at least for two reasons. First, the diffusion coefficient is expected to increase significantly as magnetic turbulences become scarce, formally up to infinity outside the diffusion zone (though light cone constraints put physical upper bounds which depend on the size of the system). This actually corresponds to the transition to the ballistic regime. A quick look at Eq. (4.7) is enough to convince oneself that this implies an infinitely short diffusion timescale, *almost* always shorter than the energy-loss timescale. Second, the DM source exhibits very large gradients over the scales of interest. More simply summarized, in the absence of magnetic inhomogeneities, electrons do propagate away close to the speed of light while losing energy through IC processes; they certainly do not lose their energy at the same position. This means that the electron density should be strongly diluted outside the diffusion zone, and that Eq. (4.10) cannot be used.

Nevertheless, irrespective of the diffusion coefficient value, there is still another asymptotic case for which the propagation length $\lambda \to 0$. This actually occurs when the electron energy tends to its injected value. Even when K is large, $\lambda \overset{E\to E_s}{\longrightarrow} 0$. This regime leads to a Green function similar to that in Eq. (4.9) except for the energy description:

$$\mathcal{G}_{E\to E_s}(E,\vec{x} \leftarrow E_s,\vec{x}_s) = \frac{\delta^3(\vec{x}-\vec{x}_s)\,\theta(E+\delta E-E_s)}{b(E,\vec{x})}\,, \tag{4.11}$$

where $\delta E \to 0$, such that the electron density reads

$$\mathcal{N}_{E\to E_s}(E,\vec{x}) = \frac{1}{b(E,\vec{x})}\int_E^{E+\delta E} dE_s \mathcal{Q}(E_s,\vec{x})\,. \tag{4.12}$$

This expression is valid outside the diffusion zone as long as the physics at stake can be described by the transport equation given in Eq. (4.1). We will discuss this into more details in a forthcoming dedicated study.

We note that in both Eqs. (4.9) and (4.11), a normalization factor of $1/b(E,\vec{x}) \approx (\tau_l(\vec{x})/E_0)(E/E_0)^{-2}$ appears, showing the strong impact of the *local* energy loss rate on the amplitude of the electron density in this limit. The spatial dependence is explicit here since we have solved the transport equation assuming $\lambda \to 0$. In contrast, the full 3D solution is valid for homogeneous losses only, as is the case for complete analytic solutions accounting for spatial boundary conditions. Since losses are more important in the Galactic disk (presence of the magnetic field and other ISRF components) than outside, we may therefore expect an electron density asymptotically slightly larger outside the disk than at the Earth's location. The spatial dependence of energy losses should therefore be properly taken into account, since impacting both the target IC photon density and the electron density. This makes the full 3D case or other Fourier-Bessel expansions formally inappropriate, though averaging the energy losses over the relevant value of λ provides a good approximation to a complete numerical treatment [72, 73].

4.3 Attempts for modeling transport beyond the diffusion slab

Some efforts have already been overtaken to study the impact of those cosmic rays injected outside the diffusion zone (see *e.g.* [74–76]). Refs. [74, 76] treat the antiproton case, for which energy losses are almost irrelevant, which makes it difficult to compare with the present configuration. On the other hand, Ref. [75] addresses the positron case with a 3-zone propagation model, where the usual diffusion zone is embedded into a vertically more extended region characterized by a much larger diffusion coefficient. Nevertheless, energy losses are taken homogeneous, which may induce some discrepancy in the high-energy limit of the electron density along the line of sight, as discussed below Eq. (4.12). Typically, the electron density should scale linearly with the energy loss timescale, which is expected to increase with the latitudinal distance until saturating to the CMB value (decrease of the magnetic field and ISRF amplitudes down to zero): a transport model with homogeneous losses normalized at the solar system's values does underpredict the asymptotic high energy electron density, and does therefore underpredict the associated IC emission[2]. This is illustrated in Fig. 3, where we compute the IC gamma-ray flux associated with the annihilation channel $\chi\chi \to e^+e^-$, with $m_\chi = 1$ TeV — we assume the DM to be smoothly distributed according to the NFW profile given in Eq. (2.1), and take a Dirac function for the injection spectrum, in contrast with the final results that will be derived by using a full Pythia [53] spectrum (which is slighly broader than the Dirac function due to Bremsstrahlung effects). The solid line is the IC flux predicted when the CMB is taken as the unique ISRF component, the dashed line corresponds to a full account of the ISRF components assumed homogeneous, while the dotted and dashed-dotted lines encodes the inhomogeneous distribution of the ISRF. We see that in the second case, the IC flux is significantly underpredicted, as discussed above. We note that a proper treatment of spatial-dependent energy losses is ensured when Eq. (4.1) is solved numerically [22, 58, 59].

Another concern comes with the angular dependence of the IC scattering cross section. Indeed, the IC flux expression given in Eq. (3.4) implicitly assumes that the incident electrons have an isotropic distribution of momenta [50–52]. Nevertheless, we may expect that when magnetic inhomogeneities get scarce, electrons are no longer isotropized, and the flux escaping from central Galactic regions is larger than the flux coming from opposite directions, as it is the case for gamma-rays. Assuming the electron flux is isotropic outside the diffusion zone will therefore likely give rise to an overestimate of the smooth halo contribution to the IC flux, since the IC scattering cross section formally depends on the scattering angle — the emitted photon is collimated along the initial electron momentum [78]. This angular effect mostly regards the smooth DM contribution, since subhalos are DM overdensities encountered along

---

[2] A remedy for local electron density computations consists in taking averaged values of the ISRF energy density [73].

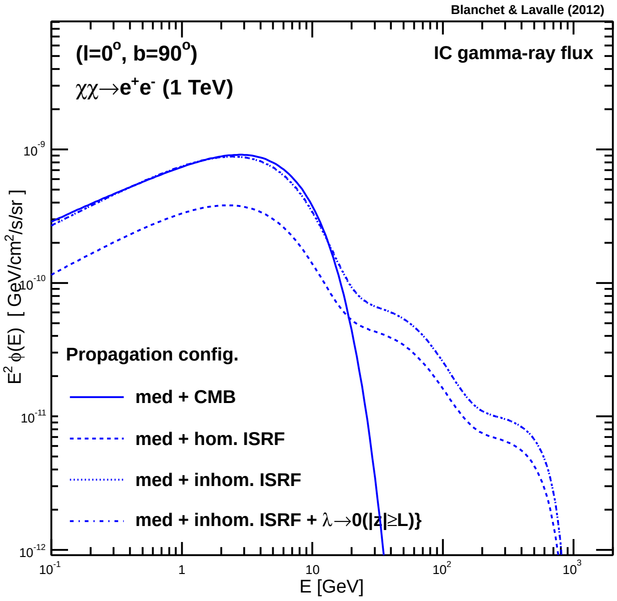

Figure 3: IC gamma-ray flux assuming annihilation into e^+e^- (1 TeV). The *med* set of propagation parameters has been adopted [67, 77]. The solid curve shows the prediction when the CMB is the only ISRF component; the dashed curve corresponds to the prediction for which all ISRF components are included but taken homogeneous in the diffusion zone; the dotted curve accounts for the spatial distribution of the ISRF; the dotted-dashed curve promotes the $E \to E_s$ regime as valid beyond the vertical boundary.

the line of sight[3]. We note that one recovers isotropy in the asymptotic regime described by Eq. (4.12), which involves electrons produced locally only.

Given the discussion above, we can adopt a tentative phenomenological approach to include the IC contributions from outside the diffusion zone as follows. We may use the slab model with usual boundary conditions (mostly the vertical one) except in the limit $\lambda \xrightarrow{E\to E_s} 0$, where we promote continuity with the outside regions by means of the asymptotic 3D solution of Eq. (4.12). Actually, as long as $\lambda \ll L$, where L is the half-height of the difussion halo, the vertical boundary has poor impact on predictions. In practice, we use a slightly modified slab model to compute the electron density up to $|z| \leq L - \epsilon$, and Eq. (4.12) otherwise. Any value of $\epsilon < 0.1$ kpc gives the same result in terms of IC gamma-ray flux. The slab model is slightly modified in the sense that we use it with the *local* value of the energy losses along the line of sight. This approximation ensures the correct asymptotic value of the electron density everywhere in the halo when $\lambda \to 0$, which is critical in the IC calculation. It is essentially correct outside the Galactic disk, while it leads to a slight underprediction of the electron density at low energies in the Galactic disk, where the star light, IR and magnetic fields concentrate. This comes from the fact that $\lambda(\vec{x}) \propto \tau_l(\vec{x})$ defines the volume inside which electrons are summed over; in the disk, τ_l is smaller than outside where one only finds the

---

[3] It is interesting to note that this anisotropy is not only characteristic of the electron flux outside the diffusion zone, but also of the ISRF fields in the disk — this is particularly relevant to compute the IC gamma-ray flux when the line of sight goes along the disk [79].

CMB component, so one integrates fewer electrons in the former case, given a DM distribution that spreads over a much larger scale. Such a physically motivated approximation is therefore very conservative, especially for low energy IC contributions. This is illustrated in Fig. 3, where the dotted-dashed line shows the consequence of promoting the $\lambda \xrightarrow{E\to E_s} 0$ regime as valid beyond the vertical boundary. The difference with the bounded case (dotted line) is hardly visible in the plot, and amounts only to a few percents.

In the following, we will adopt the so-called *med* set of propagation parameters [67, 77]. These parameters are supported by more recent constraints (*e.g.* [64]), and could even be regarded as conservative given complementary analyses which favor larger halo models (*e.g.* [80, 81]). We note that small halo models are likely already excluded since they induce secondary positrons in excess with respect to the current data [82].

We will perform a more detailed analysis dedicated to these transport issues in a forthcoming paper.

4.4 Ascribing energy Losses

Here, we summarize the way we compute the IC and synchrotron energy losses. At high energies, the dominant component is gamma-ray emission through inverse Compton scattering. The target photons can be any of the three populations (CMB, IR, SL) introduced in Sect. 2. For each population, $i =$CMB, IR, SL, we calculate the energy loss rate per electron from a full relativistic treatment [50–52]:

$$
\begin{aligned}
b_i(E,r) = 3\sigma_T \int_0^\infty \mathrm{d}E_{\rm in}\, E_{\rm in} \int_{1/4\gamma^2}^{1} \mathrm{d}q\, \frac{\mathrm{d}n_i}{\mathrm{d}E_{\rm in}}(E_{\rm in}(q),r) \frac{(4\gamma^2-\Gamma_e)q-1}{(1+\Gamma_e q)^3} \times \\
\left\{ 2q\log q + q + 1 - 2q^2 + \frac{1}{2}\frac{(\Gamma_e q)^2}{1+\Gamma_e q}(1-q) \right\} .
\end{aligned}
\tag{4.13}
$$

Compared to the emitted power in Eq. (3.3), one has to perform an additional integral over the energy of the outgoing photon, E_γ. In the Thomson regime where the incoming photon energy is much smaller than the electron mass in the electron rest frame (or, in the lab frame, $4E_{\rm in}E \ll m_e^2$), this formula simplifies substantially.

Electrons can also lose a substantial fraction of their energy through synchrotron radiation. The energy loss rate will crucially depend on the magnetic field in the Galaxy though. It is given by

$$
b_{\rm synch}(E,r) = \frac{4}{3}\frac{\sigma_T E^2}{m_e^2} u_B(r)\,, \tag{4.14}
$$

where the magnetic energy density was given in Eq. (2.4).

We show in Fig. 4 both the energy dependence and the location dependence of the energy losses experienced by electrons in our MW.

Other losses such as bremsstrahlung and ionization on interstellar matter are subdominant in the energy range of interest to us, and therefore we will not consider them here.

5 DM Subhalos

Structure formation is expected to occur hierarchically when the universe becomes matter-dominated. For WIMP-like CDM particles, for instance most of supersymmetric models,

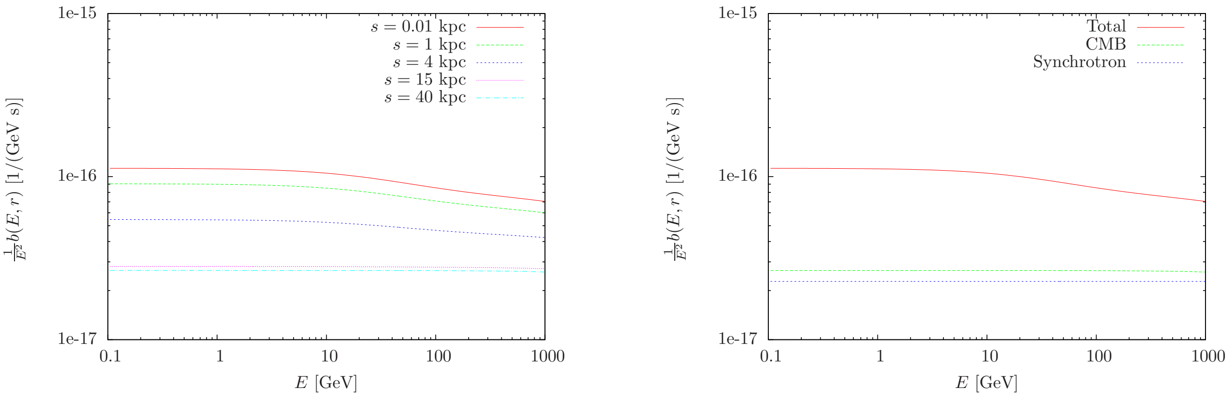

(a) (b)

Figure 4: Energy losses for an electron of energy E at different positions on the l.o.s. s towards the AGC (a), and at location $r = r_\odot$ for the different components (b).

typical free-streaming scales are such that very small structures can form, which correspond to (sub)halo masses down to 10^{-10}-10^{-4} $M_\odot$ (see *e.g.* [83, 84]).

Since formed and virialized earlier than the bigger galactic halos, in a denser universe, these tiny subhalos must be more concentrated — this is mostly a qualitative picture, since in practice, structures from the smallest to intermediate scales form almost silmutaneously. Anyway, these clumps should wander in their host galaxies in number, because they were already present at their later formation epoch or were accreted subsequently. Actually, these subhalos have long been observed on galactic scales in cosmological simulations, the most resolved of which being now able to characterize objects with masses down to $\sim 10^4\, M_\odot$ at redshift 0, with an impressive statistics amounting to hundreds of thousands of them (see the Via Lactea II [29] and Aquarius [30] suits).

The presence of a large number of subhalos has important consequences in the way predictions associated with the DM annihilation signals have to be derived. Indeed, because the annihilation rate scales with the squared DM density, the presence of inhomogeneities should increase the canonical predictions by a factor $\mathcal{B} \sim \langle n_\chi^2 \rangle / \langle n_\chi \rangle^2 > 1$, where n_χ is the DM particle number density, and the average is performed over the volume relevant to the specific detection channel [7]. This has long been recognized for the prompt emission, for which a boost factor with respect to canonical predictions was predicted, exhibiting a dependence on the angle with respect to the Galactic center (see *e.g.* [26, 33, 83, 85]). In contrast, the contribution of inverse Compton processes relies on the distribution of the DM-induced electrons, which strongly departs from the DM distribution itself because of diffusion. To our knowledge, subhalo effects have never been included for this specific case in the past, while they might have important consequences for constraining leptophilic DM models. In the following, we present the method we have adopted to include subhalos in our calculation. It is actually based on previous studies on the DM-induced antimatter signals [26, 34, 86], to which we refer the reader for more details. Indeed, we first need to calculate the electron distribution in the whole Galactic halo.

Assuming a universal DM density profile in all subhalos, the main statistical properties of the subhalo population are the mass function, the spatial distribution, and the concentration function. Here, we define the latter as $c \equiv r_{200}/r_{-2}$, where the r_{200} is the radius at which the spherically averaged subhalo density is 200 times the critical density, and r_{-2} the radius at which the logarithmic slope of the density profile equals -2. The local number density can then be expressed as

$$\begin{aligned}\frac{dN_{\rm cl}(\vec{x},M_{\rm cl})}{dV\,dM_{\rm cl}} &= \bar{N}_{\rm cl}\,\frac{d\mathcal{P}_M(\vec{x},M_{\rm cl})}{dM_{\rm cl}}\,\frac{d\mathcal{P}_V(\vec{x})}{dV}\,\frac{d\mathcal{P}_c(c,\vec{x},M_{\rm cl})}{dc} \\ &\simeq \bar{N}_{\rm cl}\,\frac{d\mathcal{P}_M(M_{\rm cl})}{dM_{\rm cl}}\,\frac{d\mathcal{P}_V(r)}{dV}\,,\end{aligned} \tag{5.1}$$

where $\bar{N}_{\rm cl}$ is the total number of subhalos in the Galaxy, and functions $\mathcal{P}$ are the probability density functions (pdfs). In the second line above, we have assumed (i) spherical symmetry, (ii) that the mass distribution is spatially homogeneous, and (iii) that the concentration parameter is fully fixed by the subhalo position and mass. The second approximation is not accurate in the very center of the Galaxy where tidal effects disrupt massive objects, a region we are not interested in in the present study, but still leads to a negligible effect in terms of global subhalo mass fraction. The third approximation cannot introduce spurious effects in the calculation of mean values, because the concentration pdf is usually found to be Gaussian for a given mass and radial position. The pdfs are all normalized to unity:

$$\begin{aligned}&\int_{M_{\rm min}}^{M_{\rm max}} dM_{\rm cl}\,\frac{d\mathcal{P}_M(M_{\rm cl})}{dM_{\rm cl}} = 1\,, \\ &\int_{\rm MW} dV\,\frac{d\mathcal{P}_V(r)}{dV} = 4\,\pi\int_0^{R_{\rm vir}} dr\,r^2\,\frac{d\mathcal{P}_V(r)}{dV} = 1\,.\end{aligned} \tag{5.2}$$

We therefore need to ascribe a spatial distribution and a mass function to the subhalo population. Following [26], we write the total mass density profile introduced in Eq. (2.1)) as the sum of a smooth component ('sm') and a clumpy one ('sub'),

$$\rho_{\rm tot}(r) = \rho_{\rm sm}(r) + \rho_{\rm sub}(r)\,. \tag{5.3}$$

Indeed, despite their limited resolution, it is reasonable to expect that the global density profiles found in current cosmological simulations, on galactic scales, will not vary in arbitrarily finer ones, though $\rho_{\rm sub}$ would be then more constrained. Assuming that subhalos carry a total MW mass fraction of $f_{\rm sub}$, that we will discuss later, integrating the previous equation leads to

$$\begin{aligned}4\pi\int_0^{R_{\rm vir}} dr\,r^2\,\rho_{\rm tot}(r) &= M_{\rm MW}\,, \\ 4\pi\int_0^{R_{\rm vir}} dr\,r^2\,\rho_{\rm sm}(r) &= (1-f_{\rm sub})\,M_{\rm MW}\,, \\ 4\pi\int_0^{R_{\rm vir}} dr\,r^2\,\rho_{\rm sub}(r) &= f_{\rm sub}\,M_{\rm MW}\,.\end{aligned} \tag{5.4}$$

If one further assumes that the smooth and subhalo components are radially antibiased, *i.e.* $\rho_{\rm sub} \propto r\,\rho_{\rm sm}$ as found in [87], then consistency with Eq. (5.3) implies that [26]

$$\rho_{\rm sm}(r) = \frac{\rho_{\rm tot}(r)}{1+r/r_b}\,, \qquad \rho_{\rm sub}(r) = \frac{\rho_{\rm tot}(r)}{1+r/r_b}\,\frac{r}{r_b}\,, \tag{5.5}$$

where r_b is the bias radius, which can easily be calculated by injecting Eq. (5.5) into Eq. (5.4).

The subhalo spatial pdf introduced in Eq. (5.1) is simply related to the substructure mass density as

$$\frac{d\mathcal{P}_V(r)}{dV} = \frac{\rho_{\rm sub}(r)}{f_{\rm sub}\,M_{\rm MW}}\,. \tag{5.6}$$

As to the mass distribution, it is usually found to be a power law consistent with the conventional Press-Schechter (PS) theory for gravitational collapse [27]. It may be expressed as

$$\frac{d\mathcal{P}_M(M_{\rm cl})}{dM_{\rm cl}}(M_{\rm cl}) = K_m \left[\frac{M_{\rm cl}}{M_\odot}\right]^{-\alpha_m} \,, \tag{5.7}$$

where K_m allows the normalization to unity inside the whole subhalo mass range:

$$K_m = \frac{1}{M_\odot} \frac{\alpha_m - 1}{\left(\frac{M_{\rm min}}{M_\odot}\right)^{1-\alpha_m} - \left(\frac{M_{\rm max}}{M_\odot}\right)^{1-\alpha_m}} \,. \tag{5.8}$$

Apart from tidal stripping effects, which are important close to the galactic center, the mass pdf does not depend on the location in the galaxy. The accurate determination of the logarithmic slope α_m is crucial for indirect dark matter searches given the broad mass range under scrutiny; values from 1.9 to 2 already induce big changes in terms of global subhalo luminosity [86]. The Press-Schechter theory predicts $\alpha_m = 2$, which is close to what is found in cosmological simulations, the most resolved of which providing values spanning the range 1.9-2 (*e.g.* [29, 30]).

To recall the bases, the PS formalism describes the collapse probability of an object of a certain size R by examining the density fluctuations on that scale. When the density contrast δ meets some critical value δ_c within a region, the mass within that region $M \propto R^3$ is assumed to collapse and virialize. Assuming the density fluctuation field is a Gaussian random variable, one can compute the collapse probability which leads to the well-know PS mass function (number density of halos per unit mass) [27]

$$\frac{dn}{dM} = \sqrt{\frac{2}{\pi}} \frac{\rho_M}{M^2} \frac{\delta_c}{\sigma_M} \left|\frac{d\ln\sigma_M}{d\ln M}\right| \exp\left(-\frac{\delta_c}{2\sigma_M^2}\right) \,, \tag{5.9}$$

where ρ_M is the mean density on the smoothing scale R, and σ_M is the mass variance. It is given by

$$\sigma_M^2(R) = \langle\delta^2(R)\rangle = \int d\ln k\, \Delta^2(k) |W(k,R)|^2 \,, \tag{5.10}$$

where $\Delta^2(k) = k^3 P(k)/(2\pi^2)$ is the dimensionless power spectrum, and $W(k,R)$ is the window function which provides the *smoothing* on a particular scale R. It is then easy to convince oneself that when $M \to 0$ (or equivalently $R \to 0$), the variance σ^2 goes to infinity, and we have the simple relation

$$\sigma_M^2(M) \propto M^{-\frac{3+n}{3}} \,, \tag{5.11}$$

where we assumed a power spectrum $P(k) \propto k^n$. Plugging into Eq. (5.9) in the limit of small masses, we have

$$\frac{dn}{dM} \propto \frac{1}{M^2} \frac{1}{\sigma_M} = \frac{1}{M^{2-\frac{3+n}{6}}} \,. \tag{5.12}$$

The PS mass function was later derived using the excursion set formalism, and it was modified by Sheth and Tormen (ST) to better match numerical simulations for the fraction of mass in collapsed objects [28]. The mass dependence in the limit $M \to 0$ then becomes

$$\frac{dn}{dM} \propto \frac{1}{M^2} \frac{1}{\sigma_M^{0.4}} = \frac{1}{M^{2-0.4\frac{3+n}{6}}} \,. \tag{5.13}$$

α_m	$M_{\rm min} = 10^{-11} M_\odot$	$M_{\rm min} = 10^{-4} M_\odot$
2	$f_{\rm sub}^{\rm tot} = 0.699$ $N_{\rm sub}^{\rm tot} = 2.66 \times 10^{21}$	$f_{\rm sub}^{\rm tot} = 0.467$ $N_{\rm sub}^{\rm tot} = 2.66 \times 10^{14}$
1.9	$f_{\rm sub}^{\rm tot} = 0.187$ $N_{\rm sub}^{\rm tot} = 3.06 \times 10^{19}$	$f_{\rm sub}^{\rm tot} = 0.181$ $N_{\rm sub}^{\rm tot} = 1.54 \times 10^{13}$

Table 2: Subhalo parameters — see the text for details.

On the smallest scales, it is well known that the power spectrum index n tends to the value -3, in which case we would have the dependence $dn/dM \propto M^{-2}$, both for the PS mass function and that of ST. This is a prediction of the PS theory on the smallest scales, which implies a scale-free distribution with a constant mass in substructure per logarithmic mass interval. However, it is unclear whether spherical collapse occurs in the same way on the smallest scales as on galactic scales. For instance, as argued in [88], when $n \to 3$ structures collapse simultaneously on a wide range of scales, and therefore they might not have time to virialize before merging or being accreted to other halos. The N-body simulations carried out in [88] seem to point in this direction, although it is too early to draw a definitive conclusion.

We provide some typical values of the total subhalo number, mass fraction, *etc.* , (see discussion above), in Tab. 2.

5.1 Prompt emission

For the prompt emission, *unresolved* subhalos are accounted for such that the l.o.s. integral of Eq. (3.1) is modified as follows (*e.g.* [26, 33, 85, 89, 90]):

$$\frac{{\rm d}\Phi}{{\rm d}E_\gamma} = \frac{r_\odot}{4\pi}\,\mathcal{S}\,\frac{{\rm d}N_\gamma}{{\rm d}E_\gamma}\int {\rm d}\Omega \int_{\rm los} \frac{{\rm d}s}{r_\odot}\,\frac{{\rm d}\mathcal{P}_V}{{\rm d}V}(r)\int_{M_{\rm min}}^{M_{\rm max}(s)} {\rm d}M_{\rm cl}\,\xi(M_{\rm cl},r)\,\frac{{\rm d}\mathcal{P}_M(M_{\rm cl})}{{\rm d}M_{\rm cl}}\,, \tag{5.14}$$

where the *local* effective annihilation volume is defined as [86]

$$\xi(M_{\rm cl},\vec{x}_s) \equiv \int_{V_{\rm sub}} {\rm d}V \left(\frac{\rho_{\rm cl}(M_{\rm cl},\vec{x}_s)}{\rho_\odot}\right)^2\,, \tag{5.15}$$

which depends on the density profile $\rho_{\rm cl}$ of the clump centered at position $\vec{x}_s$ and extending over the volume $V_{\rm cl}$. This corresponds to the volume that would provide the same global annihilation rate if the DM density inside the subhalo was taken constant and fixed to the solar value.

For an NFW profile, the annihilation volume has an analytic expression in terms of the concentration parameter c [86]:

$$\xi(M_{\rm cl},\vec{x}_s) = \frac{{M_{\rm cl}}^2}{12\pi\rho_\odot^2 r_{200}^3}\,\frac{c^4(3+c(3+c))}{(1+c)(c-(1+c)\log(1+c))^2}\,. \tag{5.16}$$

We note that a complementary approach to determine the subhalo contribution to the prompt gamma-ray emission is available in the form of a public Monte Carlo code, called CLUMPY [91].

5.2 Inverse Compton

The inverse Compton component depends crucially on the electron population coming from DM annihilation. In addition to the prompt component for which a mere line-of-sight integral is performed, here one should also include a volume integration to take into account the diffusion of these electrons and determine their density at each line-of-sight step. The electron density originating in Galactic DM clumps is then given by

$$\begin{aligned}\mathcal{N}_e^{\rm sub}(E,\vec{x}) = \mathcal{S}\int {\rm d}^3\vec{x}_s \widetilde{\mathcal{G}}_e(E,\vec{x}\leftarrow\vec{x}_s)\,\frac{{\rm d}\mathcal{P}_V}{{\rm d}V}(\vec{x}_s) \\ \times\int_{M_{\rm min}}^{M_{\rm max}} {\rm d}M_{\rm cl}\,\xi(M_{\rm cl},\vec{x}_s)\,\frac{{\rm d}\mathcal{P}_M(M_{\rm cl})}{{\rm d}M_{\rm cl}}\,, \\ \text{with}\quad \widetilde{\mathcal{G}}_e(E,\vec{x}\leftarrow\vec{x}_s)\equiv\int_E^\infty dE_s\,\mathcal{G}_e(E,\vec{x}\leftarrow E_s,\vec{x}_s)\,\frac{dN_e(E_s)}{dE_s}\,,\end{aligned} \tag{5.17}$$

which has to be substituted in Eq. (3.4) in order to find the gamma-ray flux coming from the Galactic subhalo population.

6 Results

In the previous sections, we introduced all the ingredients necessary to compute the gamma-ray flux on Earth from DM annihilation in the Galaxy. We showed how the different components make up the total flux. Annihilation can originate from the smooth Galactic DM halo, or from Galactic substructures. Moreover, photons can be produced either promptly, or via inverse Compton scattering, notably when the annihilation products involve light leptons. For the latter, we recall that we have determined the injected electron spectra by means of Pythia simulations [53], which automatically account for Bremsstrahlung processes. This implies that the spectrum associated with direct annihilation into e^+e^- is no longer described by a mere delta function.

In Fig. 5 we put everything together and show the total gamma-ray flux coming from a 1 TeV DM particle annihilating into e^+e^- (top) and $\tau^+\tau^-$ (bottom) within our Galaxy for two directions in the sky: the galactic anticenter (GAC) and the Galactic pole(s) (GP). The GAC is given by Galactic coordinates $(b,\ell)=(0,180^\circ)$, and it corresponds to the direction where the flux is expected to be the lowest. In that respect, it can be thought of as the irreducible flux for all directions. GP is defined as the direction $(90^\circ,0)$, and we choose it because the astrophysical Galactic diffuse emission (the main foreground) is best predicted and controled in this direction.

In Fig. 5 we fix the annihilation cross-section to the typical thermal relic one, $\langle\sigma v\rangle = 3\times10^{-26}$ cm^3/s, and contrast this flux with the observed IGRB obtained by Fermi-LAT with the first 10 months of data [25]. These first data extend up to 100 GeV, and we have added new preliminary data which extend the measurement of the IGRB up to 600 GeV in the Figure[92]. Note that the determination of the IGRB relies on the modeling of the diffuse emission within our Galaxy, and the identification of sources by Fermi-LAT, which are subtracted.

Looking at the upper plots of Fig. 5 we first observe that the three IC bumps are salient, corresponding, from left to right, to the electrons scattering off CMB photons, IR light, and SL. The dominant bump is clearly seen to be the CMB one. For e^+e^- we also notice that the relative contribution from IC scattering is not negligible compared to the prompt component, although the prompt emission will still dominate the exclusion limits on the annihilation cross-section we will derive below. On the other hand, for $\tau^+\tau^-$, we see that the prompt component is much more prominent than IC, and it will be clearly dominant when setting bounds on the annihilation cross-section. As discussed in the previous Section, the number of photons emitted promptly in this mode of annihilation is larger because of the hadronic component in τ decays.

Second, we find that diffusion (with *med* parameters as detailed in Sect. 4) leads to a decrease in the flux on Earth from the GP by as much as a factor of 2 at low energies, where the CMB contribution is dominant. This effect is due to the dilution of the electron density beyond the half-height of the diffusion slab (4 kpc). On the other hand, for the GAC the effect of diffusion is barely noticeable as the radius of the diffusion zone is large (20 kpc), and most of the gamma-ray signal is contained within that distance.

Finally, in order to illustrate the effect of unresolved subhalos, we show in Fig. 5 the integrated flux fixing $\alpha_m = 2$ and $M_{\rm min} = 10^{-6} M_\odot$, and we find that the flux can be enhanced by up to a factor 3 for the GP and 5 for the GAC. We also notice that this enhancement is larger for the prompt component than for IC, because the dilution effect beyond the diffusion slab mentioned above implies that only nearby substructures have an impact on the local IC gamma-ray flux — CR electrons are strongly diluted outside the diffusion zone. We will discuss the issue of transport outside the diffusion zone into more details in a forthcoming paper, where the impact of the anisotropic electron flux will be evaluated.

In Fig. 6 we illustrate the dependence of the integrated gamma-ray flux on the main subhalo parameters α_m and $M_{\rm min}$ for the DM annihilation channels e^+e^- and $\tau^+\tau^-$. We vary $M_{\rm min}$ between $10^{-11} M_\odot$ and $10^{-4} M_\odot$, which can be motivated from the point of view of the kinematic decoupling of WIMPs (for more details see [84] and references therein). Regarding the mass function index α_m we take as reference values $\alpha_m = 2$ and $\alpha_m = 1.9$, which are motivated from spherical collapse models and N-body simulations, respectively, as discussed in Sect. 5. Although these indices seem rather close, the implications for the gamma-ray flux are dramatic. With $\alpha_m = 1.9$, the signal is very marginally enhanced by the presence of subhalos, and there is a very mild dependence on the choice of minimal subhalo mass. On the other hand, for $\alpha_m = 2$, the minimal subhalo mass is crucial and the expected signal can vary by up to a factor 5. This was already emphasized in previous studies (*e.g.* [26, 86, 89, 91]). It is interesting to extract from the expected gamma-ray flux the signal enhancement when DM substructures are taken into account. Here we define the effective *boost factor* as

$$\text{Boost} \equiv \frac{{\rm d}\Phi^{\rm sub}/{\rm d}E_\gamma + {\rm d}\Phi^{\rm smooth}/{\rm d}E_\gamma}{{\rm d}\Phi^{\rm nosub}/{\rm d}E_\gamma}\,, \tag{6.1}$$

where $\Phi^{\rm sub}$ is the flux coming from subhalos (both through prompt and IC emissions), and $\Phi^{\rm smooth}$ is the flux coming from the smooth part of the DM halo. Note that the splitting between smooth and clumpy is done in a self-consistent way: as explained in detail in Sect. 5, we keep the total MW mass constant and the density profile at any radius satisfies Eq. (2.1). The result is shown in Fig. 7 for GP and the GAC. Again we vary the substructure parameters as in the previous figure. When $\alpha_m = 1.9$, we find that the signal is only enhanced by 20-30% and 30-40% for GP and the GAC, respectively, with very little dependence on $M_{\rm min}$. On the other hand, when $\alpha_m = 2$, we find that the boost can be up to a factor 20, the highest value being obtained for the prompt emission towards the GAC and for the lowest minimal subhalo mass $M_{\rm min} = 10^{-11} M_\odot$. As with Fig. 5, we notice that the boost factor for the IC component

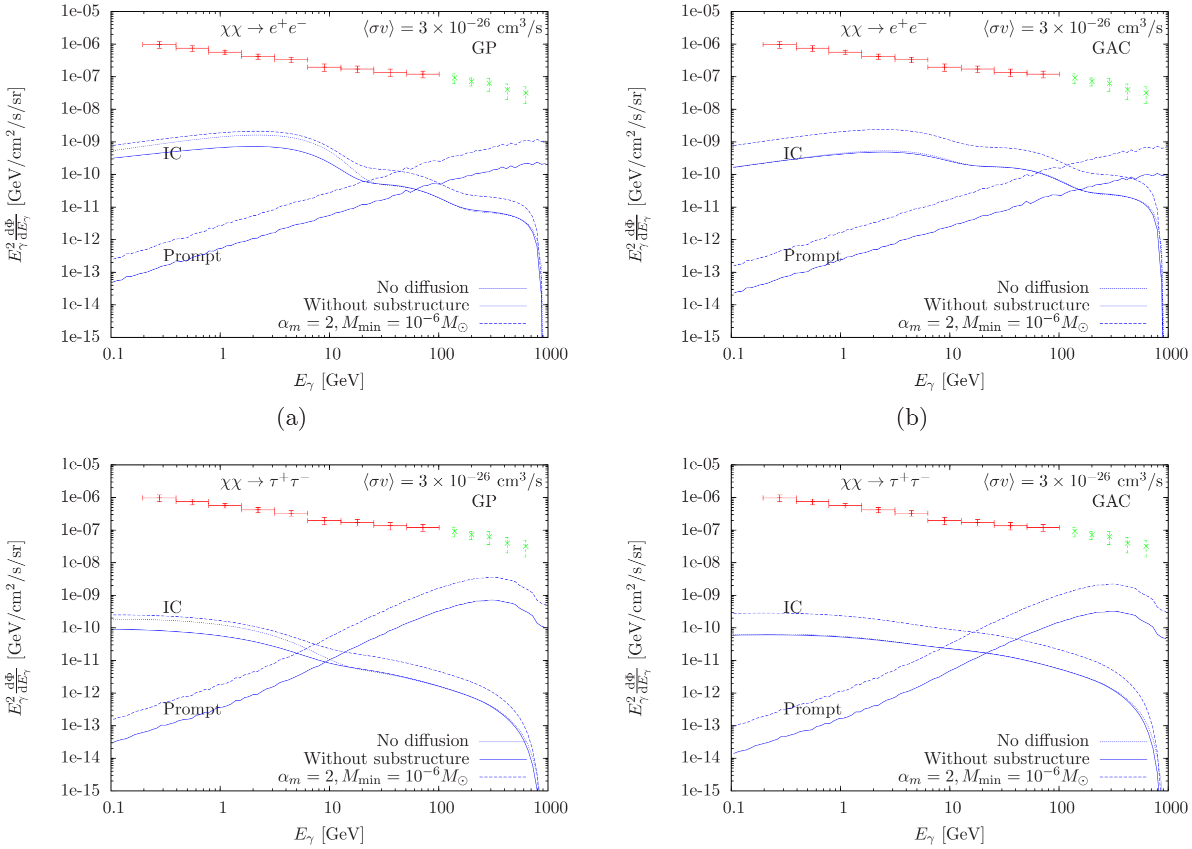

(a) (b)

(c) (d)

Figure 5: Total integrated flux for a 1 TeV DM particle annihilating into e^+e^- (top) and $\tau^+\tau^-$ (bottom) in the direction of the GAC (left) and GP (right). Shown are the IC and the prompt components, with and without boost due to subhalos.

is smaller than for the prompt one, due to the dilution effect beyond the diffusion slab, which implies that only nearby substructures contribute. Note that this effect is especially strong in the GP direction, because of the small half-height compared to the radius of the diffusion zone.

The boost has a non-trivial energy dependence which is apparent for the IC component: We can clearly see the different IC bumps as in the figures depicting the total integrated flux. The largest boost is always linked to the CMB bump, because this is where the diffusion length is the largest, and therefore the integration volume includes more substructures. On the other hand, the boost for the prompt signal is, as already well established [93], independent of energy. We also notice by comparing panels (a) and (b) of Fig. 7 that the boost factor is always larger in the case of the GAC compared to GP. The reason is that the relative mass domination of the subhalo component is reached faster towards the GAC (the line-of-sight variable $s = r - r_\odot$), than towards the GP ($s = \sqrt{r^2 - r_\odot^2}$), and therefore the boost is correspondingly larger. This is important as it implies that unresolved substructures tend to render the global signal more isotropic than a purely smooth one, as noticed in [18] for instance. In our case, the signal from the GAC is the lowest of all directions, but it is partially

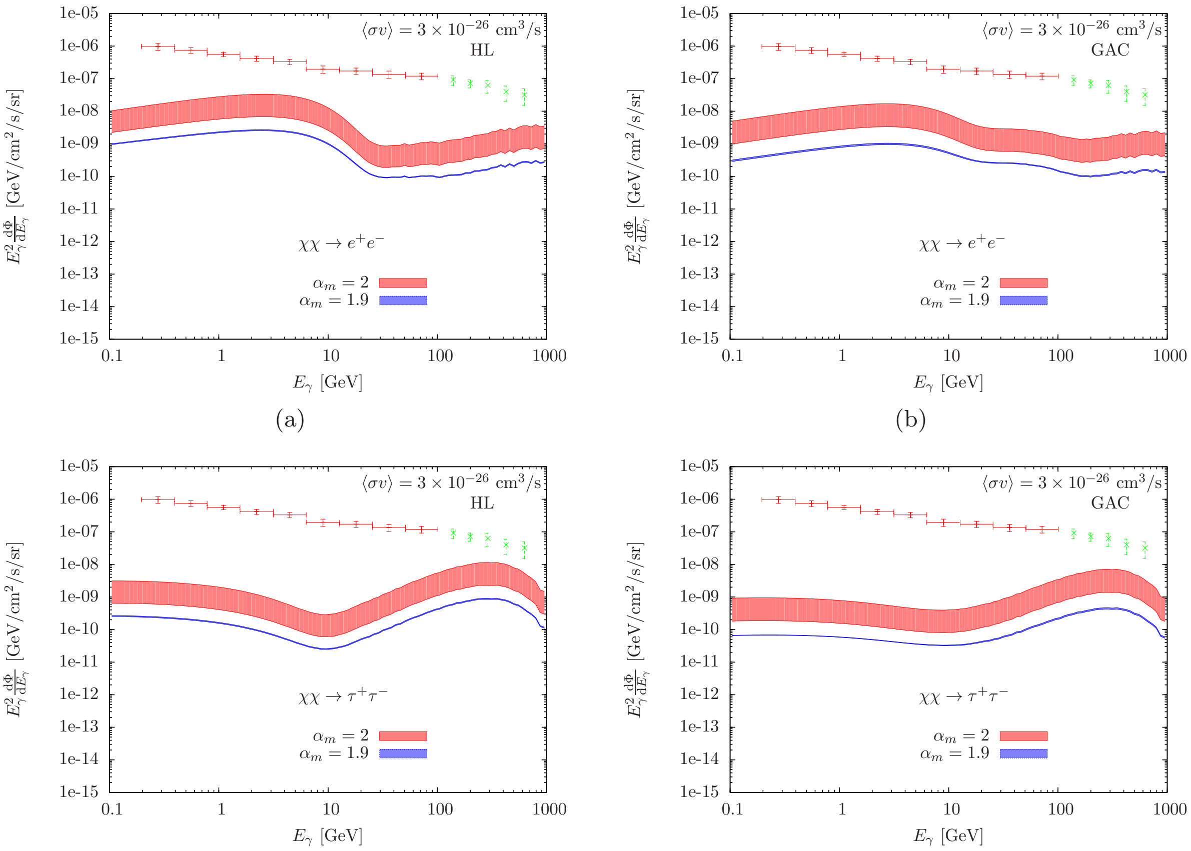

(a) (b)

(c) (d)

Figure 6: Total integrated flux for a 1 TeV DM particle annihilating into e^+e^- (top) and $\tau^+\tau^-$ (bottom) including the contribution from subhalos in the direction of the GP (a) and GAC (b) and varying the minimal subhalo mass between 10^{-11} and $10^{-4}M_\odot$.

compensated by a larger boost. As it can be noticed in Fig. 6 for the band $\alpha_m = 2$, the compensation is not complete but the effect is clearly visible.

Now that we have calculated the total integrated flux from the prompt and IC components, we can establish exclusion limits on the DM annihilation cross section as a function of the WIMP mass, for different annihilation channels. We use the IGRB as our benchmark data including the preliminary data points at higher energies shown in Fig. 5 [92]. The bounds will be set at 2σ following the statistical procedure outlined in [16], which conservatively assumes that the power law behavior of the IGRB is explained by some unspecified component, which is therefore not superimposed to the DM signal. We will later see how the bounds get stronger when the DM signal is combined with an astrophysical explanation for the IGRB.

It does not come as a surprise that the strongest limits are obtained for annihilation into $\tau^+\tau^-$, as shown in the upper two plots of Fig. 8. Even when accounting for the presence of subhalos with $\alpha_m = 2$, the signal is stronger in the direction of GP than the GAC, and therefore we obtain stronger limits in this case. In particular, for GP, we notice that the typical cross-section for a thermal relic with $\alpha_m = 2$ and $M_{\rm min} \lesssim 10^{-6}M_\odot$ is disfavored in this channel up to DM masses of about 30 GeV. On the other hand, if the index is $\alpha_m = 1.9$,

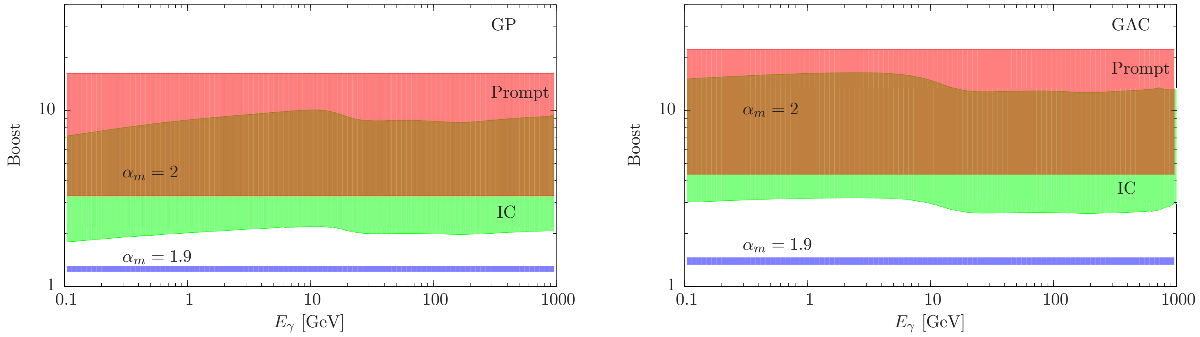

(a) (b)

Figure 7: Boost factor as a function of the energy for a 1 TeV DM particle annihilating into e^+e^-, in the direction of GP (a) and GAC (b). The colored regions are range of boosts obtained for the IC component varying the minimal halo mass between 10^{-11} and $10^{-4}M_\odot$, and for $\alpha_m = 2$ and $\alpha_m = 1.9$. The dashed lines show for comparison the range of boosts obtained for the prompt contribution in the case $\alpha_m = 2$.

the thermal relic cross-section is not excluded for any mass.

The channel $b\bar{b}$ is displayed under the $\tau^+\tau^-$ case in Fig. 8, and one can see that it is also partially constrained down to the thermal relic cross-section at low DM masses when $\alpha_m = 2$. On the other hand, the leptonic channels e^+e^-, $\mu^+\mu^-$ never reach the thermal relic cross-section, even for $\alpha_m = 2$. However, in the case $\mu^+\mu^-$, it can be seen that the regions favored to explain the PAMELA [48] and Fermi-LAT [49] excesses are marginally allowed when $\alpha_m = 1.9$ and disfavored when $\alpha_m = 2$. Note that we rescaled the regions found in [15] in order to account for a different local DM density $\rho_\odot = 0.395$ GeV/cm^3 vs. 0.3 GeV/cm^3. On the other hand, we did not account for a potential boost factor of the electron-positron flux due to substructures, which would move the regions by a factor 2-3 downwards in the case $\alpha_m = 2$ (no change when $\alpha_m = 1.9$) [26].

We now comment on the relative importance of the prompt vs. IC emission for the limits. It is clear that the hadronic channels $\tau^+\tau^-$ and $b\bar{b}$ are heavily dominated by the prompt emission. But also in the purely leptonic cases the prompt component dominates the signal and therefore the bounds all the way up to 600 GeV, leaving little room for IC. This is especially true for GP, but even for the GAC the IC contribution is subdominant as can be clearly seen in the lowest right panel of Fig. 8 corresponding to annihilation into $\mu^+\mu^-$. In previous works [16, 17, 20, 21], the IC component was clearly dominating the exclusion limits above 500 GeV. This discrepancy is easily explained by the choice of data sets. With only data published by Fermi-LAT collaboration in [25] we have indeed that the prompt component does not give a strong bound for DM masses above 500 GeV, because the flux peaks far beyond the energy range of this data set. However, including the preliminary data up to 600 GeV implies that the prompt component is dominant up to higher energies.

A comparison with previous works is now in order. As we mentioned earlier, a direct comparison is often complicated because exclusion limits are often extracted with different assumptions: including galactic and/or extragalactic contribution, with different data sets or directions in the sky, and finally the exclusion limits sometimes refer to 1σ, 2σ or 99% C.L. In the study made by the Fermi collaboration [18] only the extragalactic signal from DM annihilation was used to derive limits. The data set was the IGRB [25]. Compared to the

95% C.L. found in their work, our limits for $\alpha_m = 1.9$ are close to their reference conservative limit (MSII-Sub1). As we can see in Fig. 8, our best limits in the case $\alpha_m = 2$ are about one order of magnitude lower, which makes them slightly stronger than the case denoted by 'BulSub' in [18]. Note however that the cosmological signal from DM annihilation is even more sensitive to the DM substructure distribution than the galactic signal, as it can vary by up to three orders of magnitude (see for instance Fig. 1 in [18]) compared to one order of magnitude in our case.

In [21], the galactic signal in the direction of the galactic anticenter was considered, and compared to the IGRB. If one considers that their limits follow from the choice of a boost factor of 3.3 in our Galaxy, we obtain consistent results. In [20], both the galactic and extragalactic signal was computed and compared to the IGRB. Although no subhalo enhancement was included for the Galactic contribution, it was found to be typically dominant over the extragalactic one except for rather extreme concentration models. We obtain consistent results with this work when neglecting subhalo boost.

To date, the robust limits in the field of DM indirect detection with photons which are strongest at low DM masses are those obtained from a combined analysis of the DM signal from a set of Dwarf Spheroidal galaxies which are satellites of our MW [94]. There it was found that the thermal relic cross-section for a WIMP was starting to be excluded for low masses in the channels $\tau^+\tau^-$ and $b\bar{b}$. Their result is slightly better than our best limits in the direction of GP with the most favorable choice of parameters ($\alpha_m = 2$ and $M_{\rm min} = 10^{-11} M_\odot$). Note that our limits are more constraining at higher masses $M_\chi > 100$ GeV because we are using the additional preliminary data points of [92].

The limits on DM annihilation cross-sections shown in Fig. 8 were obtained in a conservative way. Although the shape of the DM signal is unlikely to resemble the power law spectrum of the IGRB, we did not try to superimpose a model for the IGRB in order to derive bounds on DM annihilation cross-sections. A few astrophysical sources were shown to be potentially at the origin of (at least a part of) the IGRB, most prominently blazars [95–97], non-blazar Active Galactic Nuclei (AGN) [98], star-forming galaxies [99] and milli-second pulsars [100]. It is likely that a combination of some of these contributions explains the totality of the IGRB. Here we follow the work of [97], where unresolved blazars and AGN are able to account for the IGRB. In that work, it was predicted that a substantial fraction of the as-yet unresolved blazars can be resolved after five years of data taking, yielding a potential new *measurement* of the IGRB by the Fermi collaboration, assuming a particular scaling of error bars [21]. Here we use this forecast IGRB in order to derive more stringent (though more speculative) exclusion limits for DM annihilation cross-sections. The result is shown in Fig. 9 for the case of DM annihilating into $\tau^+\tau^-$, and for the direction of GP. The limits get a factor 2-3 stronger than in Fig. 8, with masses up to 100 GeV excluded if $\alpha_m = 2$ and $M_{\rm min} = 10^{-11} M_\odot$.

We saw in the upper panels of Fig. 8 that if DM annihilates mainly in channels $\tau^+\tau^-$ or $b\bar{b}$ light masses are excluded when $\alpha_m = 2$ and the minimal halo mass is $\lesssim 10^{-6} M_\odot$. This means that in these channels we have an interesting connection between the DM mass and the mass function index α_m. We can thus exclude part of the parameter space (M_χ, α_m), as shown in Fig. 10 for the case $\tau^+\tau^-$ in the direction of GP. It can be seen that a substantial fraction of the parameter space is excluded at 2σ, especially when the minimal halo mass is as small as $10^{-11} M_\odot$. Therefore, if we came to know the DM mass from the Large Hadron Collider, and that it mainly annihilates into hadronic channels such as $\tau^+\tau^-$ or $b\bar{b}$, we would learn something important about the mass function, which is a central concept in the theory of structure formation. Conversely, if the mass function for our galaxy is determined more accurately with N-body simulations, and the extrapolation down to small halo masses is on a stronger footing, we would obtain a robust exclusion of hadronic final states at low DM masses, depending on the value of the mass function index found.

7 Conclusions

We discussed gamma-ray signals from DM annihilations in our Galaxy. We paid particular attention to the following aspects which were neglected in previous analyses: 1) when DM annihilates into light leptons, the diffusion of the electrons/positrons before IC scattering is potentially important, and 2) substructures within our Galaxy can give an additional contribution to the signal. We have first shown that diffusion only plays a subleading role in the calculation of gamma-ray fluxes on Earth for the two directions in the sky which we were interested in, namely high latitudes and the galactic anticenter — the prompt emission is almost always dominant.

Second, we have quantified the uncertainty in the gamma-ray signal due to the presence of substructures in our Galaxy. In order to choose realistic parameters for the substructure distribution, we used results from the latest N-body simulations, as well as some theoretical arguments. This lead us to choose a mass function index for our Galaxy between 1.9 and 2. Concerning the other important parameter to determine the substructure boost, namely the minimal halo mass, we vary over a wide range of values which can be motivated by the kinetic decoupling temperature of different DM particles. We found that under optimistic assumptions about both the minimal halo mass and the mass function index, the signal can be enhanced by a factor 2-20, whereas with very conservative assumptions it could be as low as 20-30%. Therefore, we have a theoretical uncertainty of roughly an order of magnitude in the prediction of the flux from DM annihilation. This can be found to be enormous, but it is much less than the uncertainty in the prediction of the extragalactic signal, which can vary by three orders of magnitude.

In order to set exclusion limits on annihilation cross-sections, we used the Isotropic Gamma-Ray Background measurement by Fermi-LAT. In the most optimistic subhalo scenario, we obtain limits that are as stringent as those derived from Dwarf-Spheroidals [94, 101, 102], with the low mass region $M_\chi < 30$ GeV excluded in the channel $\tau^+\tau^-$.

Finally, we have shown that there exists an interesting connection between the mass function index and the DM mass. In case of determination of the DM mass at a collider, and provided the main annihilation channel is known to be hadronic, we will learn something about the mass function index from the non-observation of DM signals in Fermi-LAT data.

Acknowledgments

We would like to thank Oleg Ruchayskiy and Kevork Abazajian for useful discussions. SB acknowledges support from the Swiss National Science Foundation, under the Ambizione grant PZ00P2_136947. JL wishes to thank the CFP Théorie-IN2P3 for financial support.

References

[1] V. Trimble, *Existence and nature of dark matter in the universe*, *Ann. Rev. Astron. Astroph.* **25** (1987) 425–472.

[2] T. P. Walker, G. Steigman, H.-S. Kang, D. M. Schramm, and K. A. Olive, *Primordial nucleosynthesis redux*, *Astrophys. J.* **376** (July, 1991) 51–69.

[3] E. Komatsu, K. M. Smith, J. Dunkley, *et. al.*, *Seven-year Wilkinson Microwave Anisotropy Probe (WMAP) Observations: Cosmological Interpretation*, *Astrophys. J. Suppl. Series* **192** (Feb., 2011) 18, [`arXiv:1001.4538`].

[4] J. R. Primack, D. Seckel, and B. Sadoulet, *Detection of cosmic dark matter*, *Annual Review of Nuclear and Particle Science* **38** (1988) 751–807.

[5] G. Jungman, M. Kamionkowski, and K. Griest, *Supersymmetric dark matter*, *Phys. Rept.* **267** (Mar., 1996) 195–373, [`hep-ph/9506380`].

[6] J. R. Primack, *Cosmology: small-scale issues*, *New Journal of Physics* **11** (Oct., 2009) 105029, [`arXiv:0909.2247`].

[7] J. Silk and A. Stebbins, *Clumpy cold dark matter*, *Astrophys. J.* **411** (July, 1993) 439–449.

[8] J. E. Gunn, B. W. Lee, I. Lerche, D. N. Schramm, and G. Steigman, *Some astrophysical consequences of the existence of a heavy stable neutral lepton*, *Astrophys. J.* **223** (Aug., 1978) 1015–1031.

[9] J. Silk and M. Srednicki, *Cosmic-ray antiprotons as a probe of a photino-dominated universe*, *Physical Review Letters* **53** (Aug., 1984) 624–627.

[10] L. M. Krauss, K. Freese, D. N. Spergel, and W. H. Press, *Cold dark matter candidates and the solar neutrino problem*, *Astrophys. J.* **299** (Dec., 1985) 1001–1006.

[11] W. B. Atwood *et. al.*, *The Large Area Telescope on the Fermi Gamma-Ray Space Telescope Mission*, *Astrophys. J.* **697** (June, 2009) 1071–1102, [`arXiv:0902.1089`].

[12] T. Bringmann, X. Huang, A. Ibarra, S. Vogl, and C. Weniger, *Fermi LAT Search for Internal Bremsstrahlung Signatures from Dark Matter Annihilation*, *ArXiv e-prints* (Mar., 2012) [`arXiv:1203.1312`].

[13] C. Weniger, *A Tentative Gamma-Ray Line from Dark Matter Annihilation at the Fermi Large Area Telescope*, *ArXiv e-prints* (Apr., 2012) [`arXiv:1204.2797`].

[14] M. Cirelli and P. Panci, *Inverse Compton constraints on the Dark Matter $e^{\pm}$ excesses*, *Nuclear Physics B* **821** (Nov., 2009) 399–416, [`arXiv:0904.3830`].

[15] P. Meade, M. Papucci, A. Strumia, and T. Volansky, *Dark Matter interpretations of the e excesses after FERMI*, *Nuclear Physics B* **831** (May, 2010) 178–203, [`arXiv:0905.0480`].

[16] M. Papucci and A. Strumia, *Robust implications on dark matter from the first FERMI sky γ map*, *JCAP* **3** (Mar., 2010) 14, [`arXiv:0912.0742`].

[17] M. Cirelli, P. Panci, and P. D. Serpico, *Diffuse gamma ray constraints on annihilating or decaying Dark Matter after Fermi*, *Nuclear Physics B* **840** (Nov., 2010) 284–303, [`arXiv:0912.0663`].

[18] A. A. Abdo *et. al.*, *Constraints on cosmological dark matter annihilation from the Fermi-LAT isotropic diffuse gamma-ray measurement*, *JCAP* **4** (Apr., 2010) 14, [`arXiv:1002.4415`].

[19] K. N. Abazajian, P. Agrawal, Z. Chacko, and C. Kilic, *Conservative constraints on dark matter from the Fermi-LAT isotropic diffuse gamma-ray background spectrum*, *JCAP* **11** (Nov., 2010) 41, [`arXiv:1002.3820`].

[20] G. Hütsi, A. Hektor, and M. Raidal, *Implications of the Fermi-LAT diffuse gamma-ray measurements on annihilating or decaying dark matter*, *JCAP* **7** (July, 2010) 8, [`arXiv:1004.2036`].

[21] K. N. Abazajian, S. Blanchet, and J. P. Harding, *Current and future constraints on dark matter from prompt and inverse-Compton photon emission in the isotropic diffuse gamma-ray*

background, *Phys. Rev. D* **85** (Feb., 2012) 043509, [arXiv:1011.5090].

[22] M. Cirelli, G. Corcella, A. Hektor, G. Hütsi, M. Kadastik, P. Panci, M. Raidal, F. Sala, and A. Strumia, *PPPC 4 DM ID: a poor particle physicist cookbook for dark matter indirect detection*, *JCAP* **3** (Mar., 2011) 51, [arXiv:1012.4515].

[23] K. N. Abazajian and J. P. Harding, *Constraints on WIMP and Sommerfeld-enhanced dark matter annihilation from HESS observations of the galactic center*, *JCAP* **1** (Jan., 2012) 41, [arXiv:1110.6151].

[24] K. N. Abazajian, P. Agrawal, Z. Chacko, and C. Kilic, *Lower Limits on the Strengths of Gamma Ray Lines from WIMP Dark Matter Annihilation*, *ArXiv e-prints* (Nov., 2011) [arXiv:1111.2835].

[25] A. A. Abdo *et. al.*, *Spectrum of the Isotropic Diffuse Gamma-Ray Emission Derived from First-Year Fermi Large Area Telescope Data*, *Physical Review Letters* **104** (Mar., 2010) 101101, [arXiv:1002.3603].

[26] L. Pieri, J. Lavalle, G. Bertone, and E. Branchini, *Implications of high-resolution simulations on indirect dark matter searches*, *Phys. Rev. D* **83** (Jan., 2011) 023518–+, [arXiv:0908.0195].

[27] W. H. Press and P. Schechter, *Formation of Galaxies and Clusters of Galaxies by Self-Similar Gravitational Condensation*, *Astrophys. J.* **187** (Feb., 1974) 425–438.

[28] R. K. Sheth, H. J. Mo, and G. Tormen, *Ellipsoidal collapse and an improved model for the number and spatial distribution of dark matter haloes*, *MNRAS* **323** (May, 2001) 1–12, [astro-ph/9907024].

[29] J. Diemand, M. Kuhlen, P. Madau, M. Zemp, B. Moore, D. Potter, and J. Stadel, *Clumps and streams in the local dark matter distribution*, *Nature* **454** (Aug., 2008) 735–738, [arXiv:0805.1244].

[30] V. Springel, J. Wang, M. Vogelsberger, A. Ludlow, A. Jenkins, A. Helmi, J. F. Navarro, C. S. Frenk, and S. D. M. White, *The Aquarius Project: the subhaloes of galactic haloes*, *MNRAS* **391** (Dec., 2008) 1685–1711, [arXiv:0809.0898].

[31] J. Diemand, B. Moore, and J. Stadel, *Earth-mass dark-matter haloes as the first structures in the early Universe*, *Nature* **433** (Jan., 2005) 389–391, [astro-ph/0501589].

[32] P. Ullio, L. Bergström, J. Edsjö, and C. Lacey, *Cosmological dark matter annihilations into γ rays: A closer look*, *Phys. Rev. D* **66** (Dec., 2002) 123502–+, [astro-ph/0207125].

[33] L. Bergström, J. Edsjö, P. Gondolo, and P. Ullio, *Clumpy neutralino dark matter*, *Phys. Rev. D* **59** (Feb., 1999) 043506, [astro-ph/9806072].

[34] J. Lavalle, J. Pochon, P. Salati, and R. Taillet, *Clumpiness of dark matter and the positron annihilation signal*, *Astron. Astroph.* **462** (Feb., 2007) 827–840, [astro-ph/0603796].

[35] P. Madau, J. Diemand, and M. Kuhlen, *Dark Matter Subhalos and the Dwarf Satellites of the Milky Way*, *Astrophys. J.* **679** (June, 2008) 1260–1271, [arXiv:0802.2265].

[36] The Fermi-LAT Collaboration, *Fermi-LAT Observations of the Diffuse Gamma-Ray Emission: Implications for Cosmic Rays and the Interstellar Medium*, *ArXiv e-prints* (Feb., 2012) [arXiv:1202.4039].

[37] J. F. Navarro, C. S. Frenk, and S. D. M. White, *A Universal Density Profile from Hierarchical Clustering*, *Astrophys. J.* **490** (Dec., 1997) 493–+, [astro-ph/9611107].

[38] P. J. McMillan, *Mass models of the Milky Way*, *MNRAS* **414** (July, 2011) 2446–2457, [arXiv:1102.4340].

[39] R. Catena and P. Ullio, *A novel determination of the local dark matter density*, *JCAP* **8** (Aug., 2010) 4–+, [arXiv:0907.0018].

[40] P. Salucci, F. Nesti, G. Gentile, and C. Frigerio Martins, *The dark matter density at the Sun's location*, *Astron. Astroph.* **523** (Nov., 2010) A83+, [arXiv:1003.3101].

[41] J. Bovy and S. Tremaine, *On the local dark matter density*, *ArXiv e-prints* (May, 2012) [arXiv:1205.4033].

[42] T. A. Porter and et al., *A new estimate of the Galactic interstellar radiation field between 0.1um and 1000um*, in *International Cosmic Ray Conference*, vol. 4 of *International Cosmic Ray Conference*, pp. 77–+, 2005.

[43] T. Shibata, T. Ishikawa, and S. Sekiguchi, *A Possible Approach to Three-dimensional Cosmic-ray Propagation in the Galaxy. IV. Electrons and Electron-induced γ-rays*, *Astrophys. J.* **727** (Jan., 2011) 38–+, [arXiv:1010.5652].

[44] A. W. Strong, I. V. Moskalenko, and O. Reimer, *Diffuse Continuum Gamma Rays from the Galaxy*, *Astrophys. J.* **537** (July, 2000) 763–784, [astro-ph/9811296].

[45] J. F. Beacom, N. F. Bell, and G. Bertone, *Gamma-Ray Constraint on Galactic Positron Production by MeV Dark Matter*, *Physical Review Letters* **94** (May, 2005) 171301–+, [astro-ph/0409403].

[46] A. Ibarra and D. Tran, *Decaying dark matter and the PAMELA anomaly*, *JCAP* **2** (Feb., 2009) 21, [arXiv:0811.1555].

[47] A. Ibarra, D. Tran, and C. Weniger, *Decaying dark matter in light of the PAMELA and Fermi LAT data*, *JCAP* **1** (Jan., 2010) 9, [arXiv:0906.1571].

[48] O. Adriani *et. al.*, *An anomalous positron abundance in cosmic rays with energies 1.5-100GeV*, *Nature* **458** (Apr., 2009) 607–609, [arXiv:0810.4995].

[49] A. A. Abdo *et. al.*, *Measurement of the Cosmic Ray $e^+ + e^-$ Spectrum from 20GeV to 1TeV with the Fermi Large Area Telescope*, *Physical Review Letters* **102** (May, 2009) 181101–+, [arXiv:0905.0025].

[50] F. C. Jones, *Inverse Compton Scattering of Cosmic-Ray Electrons*, *Physical Review* **137** (Mar., 1965) 1306–1311.

[51] F. C. Jones, *Calculated Spectrum of Inverse-Compton-Scattered Photons*, *Physical Review* **167** (Mar., 1968) 1159–1169.

[52] G. R. Blumenthal and R. J. Gould, *Bremsstrahlung, Synchrotron Radiation, and Compton Scattering of High-Energy Electrons Traversing Dilute Gases*, *Reviews of Modern Physics* **42** (1970) 237–271.

[53] T. Sjöstrand, S. Mrenna, and P. Skands, *PYTHIA 6.4 physics and manual*, *Journal of High Energy Physics* **5** (May, 2006) 26–+, [hep-ph/0603175].

[54] S. I. Syrovatskii, *The Distribution of Relativistic Electrons in the Galaxy and the Spectrum of Synchrotron Radio Emission.*, *Sov. Astron.* **3** (Feb., 1959) 22.

[55] V. L. Ginzburg and S. I. Syrovatskii, *The Origin of Cosmic Rays.* New York: Macmillan, 1964.

[56] V. S. Berezinskii, S. V. Bulanov, V. A. Dogiel, and V. S. Ptuskin, *Astrophysics of cosmic rays.* Amsterdam: North-Holland, edited by Ginzburg, V.L., 1990.

[57] T. Delahaye, F. Donato, N. Fornengo, J. Lavalle, R. Lineros, P. Salati, and R. Taillet, *Galactic secondary positron flux at the Earth*, *Astron. Astroph.* **501** (July, 2009) 821–833, [arXiv:0809.5268].

[58] A. W. Strong and I. V. Moskalenko, *Propagation of Cosmic-Ray Nucleons in the Galaxy*, *Astrophys. J.* **509** (Dec., 1998) 212–228, [astro-ph/9807150].

[59] G. Di Bernardo, C. Evoli, D. Gaggero, D. Grasso, and L. Maccione, *Unified interpretation of*

cosmic-ray nuclei and antiproton recent measurements, *ArXiv e-prints* (Sept., 2009) [arXiv:0909.4548].

[60] S. V. Bulanov and V. A. Dogel, *The Influence of the Energy Dependence of the Diffusion Coefficient on the Spectrum of the Electron Component of Cosmic Rays and the Radio Background Radiation of the Galaxy*, *APSS* **29** (Aug., 1974) 305–318.

[61] E. A. Baltz and J. Edsjö, *Positron propagation and fluxes from neutralino annihilation in the halo*, *Phys. Rev. D* **59** (Jan., 1998) 023511, [astro-ph/9808243].

[62] F. Casse, M. Lemoine, and G. Pelletier, *Transport of cosmic rays in chaotic magnetic fields*, *Phys. Rev. D* **65** (Jan., 2002) 023002, [astro-ph/0109223].

[63] A. Shalchi, *Nonlinear Cosmic Ray Diffusion Theories*. Springer, 2009.

[64] A. Putze, L. Derome, and D. Maurin, *A Markov Chain Monte Carlo technique to sample transport and source parameters of Galactic cosmic rays. II. Results for the diffusion model combining B/C and radioactive nuclei*, *Astron. Astroph.* **516** (June, 2010) A66+, [arXiv:1001.0551].

[65] A. A. Abdo *et. al.*, *Fermi Large Area Telescope Measurements of the Diffuse Gamma-Ray Emission at Intermediate Galactic Latitudes*, *Physical Review Letters* **103** (Dec., 2009) 251101–+.

[66] J. Lavalle, *10 GeV dark matter candidates and cosmic-ray antiprotons*, *Phys. Rev. D* **82** (Oct., 2010) 081302–+, [arXiv:1007.5253].

[67] F. Donato, N. Fornengo, D. Maurin, P. Salati, and R. Taillet, *Antiprotons in cosmic rays from neutralino annihilation*, *Phys. Rev. D* **69** (Mar., 2004) 063501–+, [astro-ph/0306207].

[68] T. Delahaye, R. Lineros, F. Donato, N. Fornengo, and P. Salati, *Positrons from dark matter annihilation in the galactic halo: Theoretical uncertainties*, *Phys. Rev. D* **77** (Mar., 2008) 063527–+, [arXiv:0712.2312].

[69] J. Lavalle and P. Salati, *Dark Matter Indirect Signatures*, *ArXiv e-prints* (May, 2012) [arXiv:1205.1004].

[70] J. Lavalle, *Sunyaev-Zel'dovich effects from annihilating dark matter in the Milky Way: Smooth halo, subhalos, and intermediate-mass black holes*, *Phys. Rev. D* **82** (Oct., 2010) 083521–+, [arXiv:1008.5124].

[71] M. D. Kistler and J. M. Siegal-Gaskins, *Gamma-ray signatures of annihilation to charged leptons in dark matter substructure*, *Phys. Rev. D* **81** (May, 2010) 103521, [arXiv:0909.0519].

[72] D. Malyshev, I. Cholis, and J. Gelfand, *Pulsars versus dark matter interpretation of ATIC/PAMELA*, *Phys. Rev. D* **80** (Sept., 2009) 063005–+, [arXiv:0903.1310].

[73] T. Delahaye, J. Lavalle, R. Lineros, F. Donato, and N. Fornengo, *Galactic electrons and positrons at the Earth: new estimate of the primary and secondary fluxes*, *Astron. Astroph.* **524** (Dec., 2010) A51+, [arXiv:1002.1910].

[74] A. Barrau, G. Boudoul, F. Donato, D. Maurin, P. Salati, and R. Taillet, *Antiprotons from primordial black holes*, *Astron. Astroph.* **388** (June, 2002) 676–687, [astro-ph/0112486].

[75] M. Perelstein and B. Shakya, *Remarks on calculation of positron flux from galactic dark matter*, *Phys. Rev. D* **82** (Aug., 2010) 043505, [arXiv:1002.4588].

[76] M. Perelstein and B. Shakya, *Antiprotons from dark matter: Effects of a position-dependent diffusion coefficient*, *Phys. Rev. D* **83** (June, 2011) 123508, [arXiv:1012.3772].

[77] D. Maurin, F. Donato, R. Taillet, and P. Salati, *Cosmic Rays below Z=30 in a Diffusion Model: New Constraints on Propagation Parameters*, *Astrophys. J.* **555** (July, 2001) 585–596, [astro-ph/0101231].

[78] F. A. Aharonian and A. M. Atoyan, *Compton scattering of relativistic electrons in compact X-ray sources*, *APSS* **79** (Oct., 1981) 321–336.

[79] I. V. Moskalenko and A. W. Strong, *Anisotropic Inverse Compton Scattering in the Galaxy*, *Astrophys. J.* **528** (Jan., 2000) 357–367, [astro-ph/9811284].

[80] A. W. Strong, E. Orlando, and T. R. Jaffe, *The interstellar cosmic-ray electron spectrum from synchrotron radiation and direct measurements*, *Astron. Astroph.* **534** (Oct., 2011) A54, [arXiv:1108.4822].

[81] T. Bringmann, F. Donato, and R. A. Lineros, *Radio data and synchrotron emission in consistent cosmic ray models*, *JCAP* **1** (Jan., 2012) 49, [arXiv:1106.4821].

[82] J. Lavalle, *Impact of the spectral hardening of TeV cosmic rays on the prediction of the secondary positron flux*, *MNRAS* **414** (June, 2011) 985–991, [arXiv:1011.3063].

[83] V. Berezinsky, V. Dokuchaev, and Y. Eroshenko, *Small-scale clumps in the galactic halo and dark matter annihilation*, *Phys. Rev. D* **68** (Nov., 2003) 103003–+, [astro-ph/0301551].

[84] T. Bringmann, *Particle models and the small-scale structure of dark matter*, *New Journal of Physics* **11** (Oct., 2009) 105027–+, [arXiv:0903.0189].

[85] X.-J. Bi, *Gamma rays from the neutralino dark matter annihilations in the Milky Way substructures*, *Nuclear Physics B* **741** (May, 2006) 83–107, [astro-ph/0510714].

[86] J. Lavalle, Q. Yuan, D. Maurin, and X.-J. Bi, *Full calculation of clumpiness boost factors for antimatter cosmic rays in the light of* Λ*CDM N-body simulation results. Abandoning hope in clumpiness enhancement?*, *Astron. Astroph.* **479** (Feb., 2008) 427–452, [arXiv:0709.3634].

[87] J. Diemand, M. Kuhlen, and P. Madau, *Formation and Evolution of Galaxy Dark Matter Halos and Their Substructure*, *Astrophys. J.* **667** (Oct., 2007) 859–877, [astro-ph/0703337].

[88] P. J. Elahi, R. J. Thacker, L. M. Widrow, and E. Scannapieco, *Subhaloes in scale-free cosmologies*, *MNRAS* **395** (June, 2009) 1950–1962, [arXiv:0811.0206].

[89] L. Pieri, G. Bertone, and E. Branchini, *Dark matter annihilation in substructures revised*, *MNRAS* **384** (Mar., 2008) 1627–1637, [arXiv:0706.2101].

[90] M. Kamionkowski, S. M. Koushiappas, and M. Kuhlen, *Galactic substructure and dark-matter annihilation in the Milky Way halo*, *Phys. Rev. D* **81** (Feb., 2010) 043532, [arXiv:1001.3144].

[91] A. Charbonnier, C. Combet, and D. Maurin, *CLUMPY: A code for* γ*-ray signals from dark matter structures*, *Computer Physics Communications* **183** (Mar., 2012) 656–668, [arXiv:1201.4728].

[92] **Fermi-LAT** Collaboration, A. Morselli, *Fermi results*, *Dark Side of the Universe conference, Beijing* (2011).

[93] L. Bergström, J. Edsjö, and P. Ullio, *Cosmic Antiprotons as a Probe for Supersymmetric Dark Matter?*, *Astrophys. J.* **526** (Nov., 1999) 215–235, [astro-ph/9902012].

[94] M. Ackermann *et. al.*, *Constraining Dark Matter Models from a Combined Analysis of Milky Way Satellites with the Fermi Large Area Telescope*, *Physical Review Letters* **107** (Dec., 2011) 241302, [arXiv:1108.3546].

[95] Y. Inoue and T. Totani, *The Blazar Sequence and the Cosmic Gamma-ray Background Radiation in the Fermi Era*, *Astrophys. J.* **702** (Sept., 2009) 523–536, [arXiv:0810.3580].

[96] Y. Inoue and T. Totani, *ERRATUM: "The Blazar Sequence and the Cosmic Gamma-ray Background Radiation in the Fermi Era" ¡A href="/abs/2009ApJ...702..523I"¿(2009, ApJ, 702, 523)¡/A¿*, *Astrophys. J.* **728** (Feb., 2011) 73.

[97] K. N. Abazajian, S. Blanchet, and J. P. Harding, *Contribution of blazars to the extragalactic diffuse gamma-ray background and their future spatial resolution*, *Phys. Rev. D* **84** (Nov.,

2011) 103007, [arXiv:1012.1247].

[98] Y. Inoue, T. Totani, and Y. Ueda, *The Cosmic MeV Gamma-Ray Background and Hard X-Ray Spectra of Active Galactic Nuclei: Implications for the Origin of Hot AGN Coronae*, *Astrophys. J. Lett.* **672** (Jan., 2008) L5–L8, [arXiv:0709.3877].

[99] B. D. Fields, V. Pavlidou, and T. Prodanović, *Cosmic Gamma-ray Background from Star-forming Galaxies*, *Astrophys. J. Lett.* **722** (Oct., 2010) L199–L203, [arXiv:1003.3647].

[100] C.-A. Faucher-Giguère and A. Loeb, *The pulsar contribution to the gamma-ray background*, *JCAP* **1** (Jan., 2010) 5, [arXiv:0904.3102].

[101] A. A. Abdo *et. al.*, *Observations of Milky Way Dwarf Spheroidal Galaxies with the Fermi-Large Area Telescope Detector and Constraints on Dark Matter Models*, *Astrophys. J.* **712** (Mar., 2010) 147–158, [arXiv:1001.4531].

[102] A. Geringer-Sameth and S. M. Koushiappas, *Exclusion of Canonical Weakly Interacting Massive Particles by Joint Analysis of Milky Way Dwarf Galaxies with Data from the Fermi Gamma-Ray Space Telescope*, *Physical Review Letters* **107** (Dec., 2011) 241303, [arXiv:1108.2914].

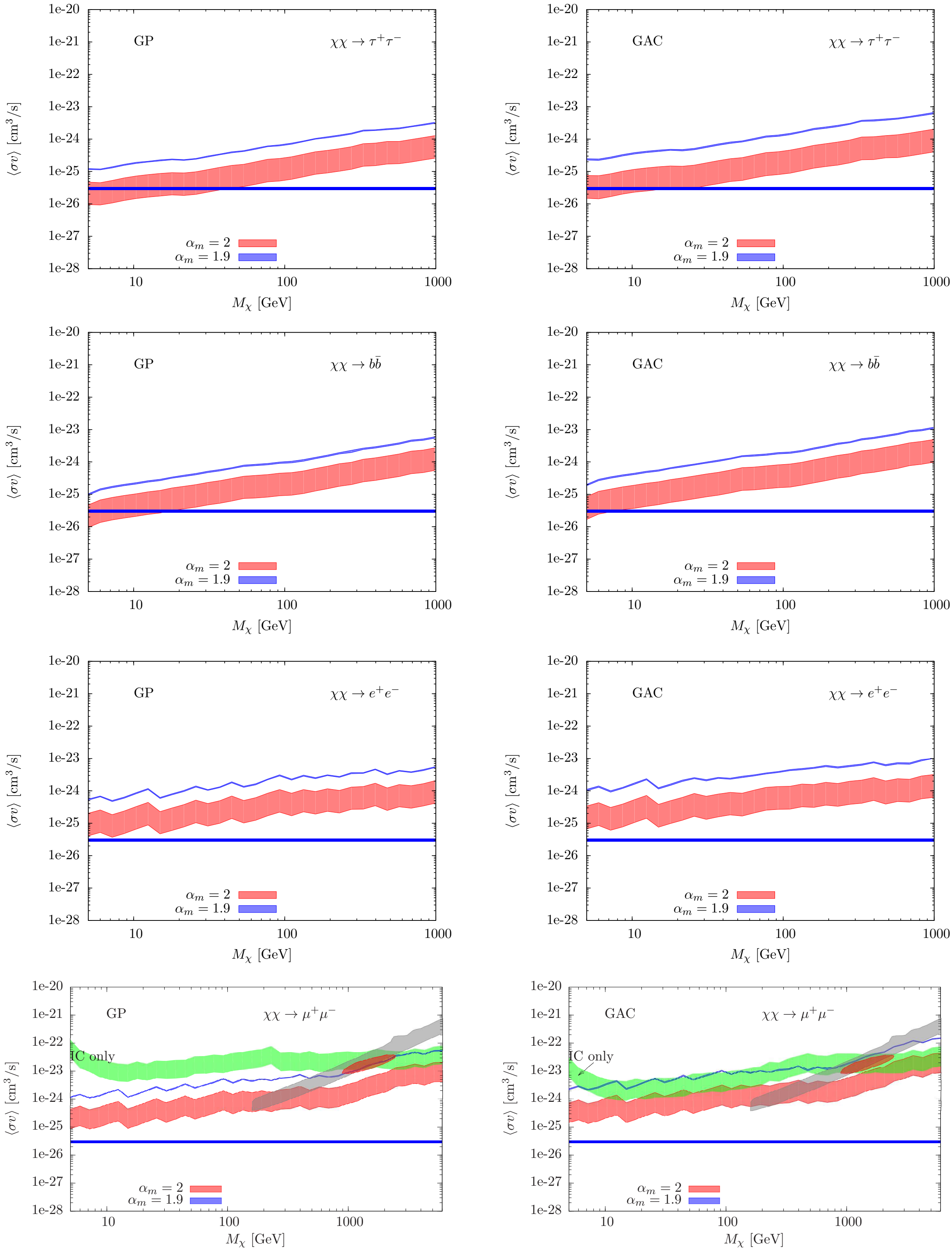

Figure 8: Limits on the thermally averaged DM annihilation cross-section for different channels, in the direction of GP (left) and GAC (right) when $\alpha_m = 2$ and $\alpha_m = 1.9$. In the bottom panels, the orange and gray ellipses represent the regions taken from [15] favored to explain the positron excess (at 3σ) by PAMELA [48] and the excess in $e^+ + e-$ seen by Fermi-LAT (5σ) [49], respectively.

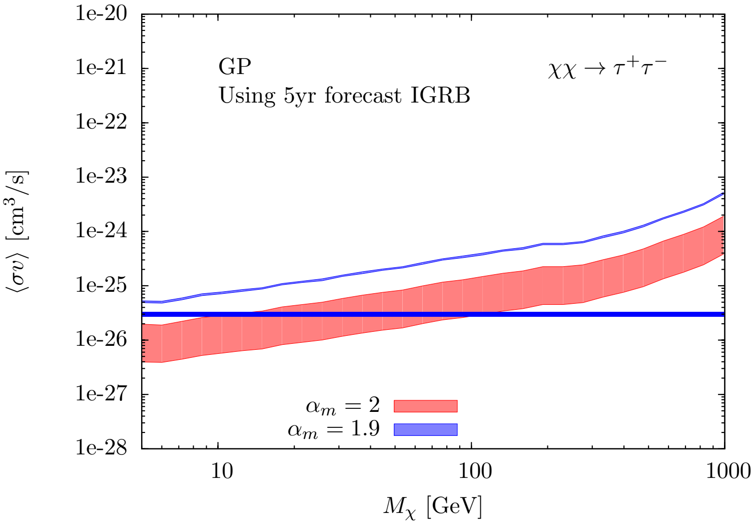

Figure 9: Tentative limits on DM annihilation cross-section for the channel $\tau^+\tau^-$ in the direction of GP using the 5yr forecast IGRB derived in [21], where unresolved blazars are assumed to make the bulk of the IGRB measured by Fermi-LAT.

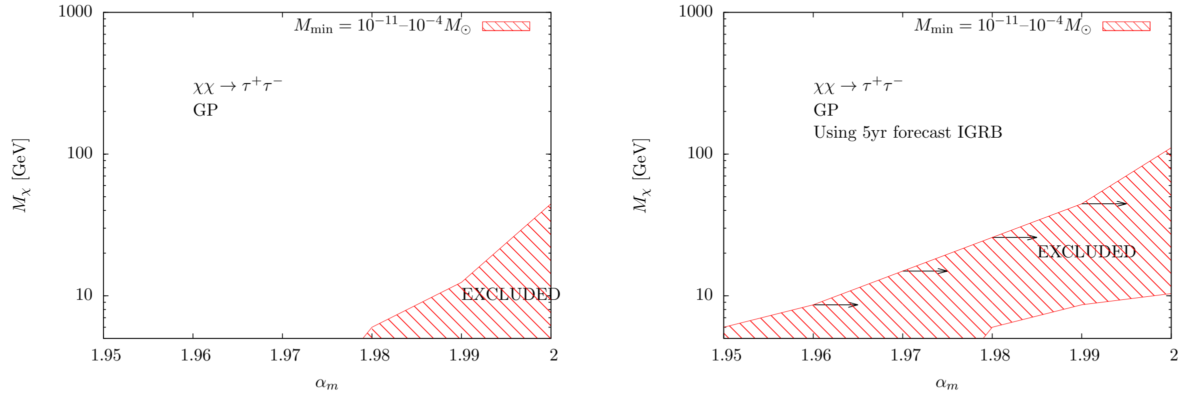

(a) (b)

Figure 10: Exclusion at 2σ in the plane (M_χ, α_m), if DM annihilates into $\tau^+\tau^-$. The left panel shows the limit using the existing IGRB, and the right one uses the forecast IGRB from [21]. The minimal halo mass $M_{\rm min}$ is varied between 10^{-11} and $10^{-4} M_\odot$.